Russian Geology and Geophysics © 2019, V.S. Sobolev IGM, Siberian Branch of the RAS
Vol. 60, No. 10, pp. 1077–1100, 2019 *DOI:10.15372/RGG2019100* *Geologiya i Geofizika*

Physicochemical Parameters of Magmatism of the Uksichan and Ichinsky Volcanoes (Sredinnyi Ridge, Kamchatka): Data on Melt Inclusions

N.L. Dobretsov[a,c,] ✉, V.A. Simonov[b,c,d], A.V. Kotlyarov[b,d], N.S. Karmanov[b]

[a]*A.A. Trofimuk Institute of Petroleum Geology and Geophysics, Siberian Branch of the Russian Academy of Sciences, pr. Akademika Koptyuga 3, Novosibirsk, 630090, Russia*

[b]*V.S. Sobolev Institute of Geology and Mineralogy, Siberian Branch of the Russian Academy of Sciences, pr. Akademika Koptyuga 3, Novosibirsk, 630090, Russia*

[c]*Novosibirsk State University, ul. Pirogova 2, Novosibirsk, 630090, Russia*

[d]*Kazan Federal University, ul. Kremlevskaya 18, Kazan, 420008, Russia*

Received 14 September 2018; received in revised form 13 December 2018; accepted 21 March 2019

Abstract—Thermobarogeochemical study of melt inclusions and investigation of clinopyroxenes and amphiboles from effusive rocks of the Uksichan and Ichinsky Volcanoes gave an insight into the parameters of deep-seated melts and the evolution of magmatic systems during the formation of minerals in intermediate chambers. Study of melt inclusions from the Uksichan volcanic rocks made it possible to estimate the pressure during the liquidus crystallization of clinopyroxenes and plagioclases from basaltic magmas and to establish four depth intervals of the formation of these minerals: ~60, 45–30, 27–18, and from 12 km to the subsurface. Comparison of the results of calculation based on melt inclusion data and of the clinopyroxene and amphibole data helped to establish the evolution paths of the *P–T* parameters of ascending melts of the Uksichan Volcano. The most high-temperature magmas, generated at a depth of ~60 km, are characterized by a successive temperature decrease during their ascent (1320–1240–1200 ºC). Based on the representative data on the compositions of amphiboles from the Uksichan and Ichinsky Volcanoes, we have elucidated the general regularities of the evolution of intermediate and acid magmatic systems, with three depths of crystallization in intermediate chambers. Amphiboles of the Ichinsky Volcano andesites and the Uksichan Volcano latites crystallized at depths of 22.0–18.5 and 18–16 km and at temperatures of 980–930 and 1010–985 ºC, respectively. As melt ascended to a depth of 15.5–11.0 km and a temperature decreased from 945 to 880 ºC, amphiboles of andesites and dacites of both volcanoes were produced. At the final stage (a temperature decrease to 900–810 ºC and ascent of melts to a depth of 3 km), only amphiboles of dacites of both volcanoes crystallized.

Keywords: physicochemical parameters of magmatism, melt inclusions, clinopyroxene, amphibole, basalt, andesite, dacite, intermediate suprasubduction chambers, volcanoes of Kamchatka

INTRODUCTION

The volcanic belt of the Sredinnyi Ridge in Kamchatka (Fig. 1) evolved as an ordinary subduction zone from 45–50 to 17–15 Ma (Gordeev and Dobretsov, 2017) and became a back-arc structure after a lull and a collision of Kamchatka with the Karaga island arc about 13–15 Ma. The belt comprises large stratovolcanoes and caldera volcanoes that have erupted abundant typically subduction-related andesite-dacite-rhyolite lavas zones coexisting with later small basaltic lava cones and fields of tuff-lava cones of subalkaline basalts common to back-arc zones.

The area has attracted much interest, but studies in two recent decades (Bindeman et al., 2004, 2010; Perepelov, 2004, 2005, 2014; Kostitsyn and Anosova, 2013; Davydova, 2014; Perepelov et al., 2016) have been limited to specific problems of magmatism, while the whole history of volcanism in the Sredinnyi Ridge remains poorly understood. In our previous publications (Dobretsov et al., 2013, 2016), typical rocks of Ichinsky Volcano, the only large active volcano in the Sredinnyi Range, were compared with the modern lavas of Tolbachik in the Klyuchevskoy group of Volcanoes. This paper presents new data on thermobarometry and mineralogy of samples from Uksichan and Ichinsky volcanoes (Figs. 2, 3) which shed light on the structure of the southern Sredinnyi Ridge belt comprising the two volcanoes and edifices between them (Fig. 3). The study aimed at updating the evolution model of volcanism in the area with the example of two large volcanoes: Uksichan and Ichinsky. The obtained new analytical data on minerals and melt inclusions from the Uksichan and Ichinsky samples were used for reference in modeling which has provided constraints on the parameters of melts and the evolution of magmatic systems leading to crystallization in intermediate magma reservoirs beneath the volcanoes. The magmatic processes in the Kamchatka Sredinnyi Ridge inferred from the obtained data on geology, petrology, geochemistry, mineralogy, and geo-

✉ Corresponding author.
E-mail adress: DobretsovNL@ipgg.sbras.ru (N.L. Dobretsov)

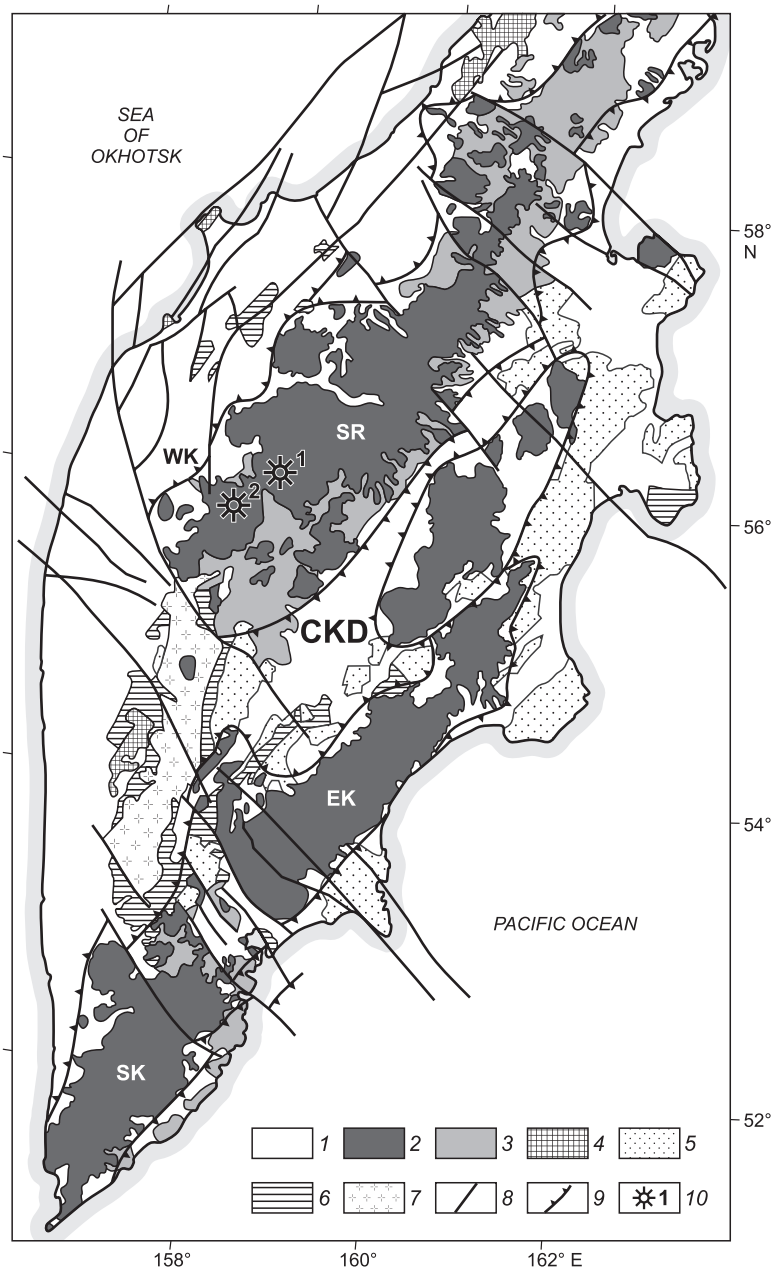

Fig. 1. Sketch map of suprasubduction magmatism in Kamchatka. *1*, modern and Neogene volcanosedimentary rocks, undifferentiated; *2*, Pliocene–Holocene volcanic belts of South Kamchatka (SK), East Kamchatka (EK) and Sredinnyi Ridge (SR); *3*, Oligocene–Miocene volcanic complexes; *4*, Early–Middle Eocene West Kamchatka volcanic belt (WK); *5*, Paleogene volcanic, volcanosedimentary, and terrigenous complexes; *6*, Late Cretaceous volcanic and terrigenous complexes; *7*, granitic gneiss domes and collisional zones; *8*, faults; *9*, boundaries of volcanic belts; *10*, sampled volcanoes Uksichan (1) and Ichinsky (2). CKD, Central Kamchatka Depression. Compiled with reference to data from (Perepelov, 2014).

thermobarometry of the Uksichan and Ichinsky samples have been additionally justified through correlation with seismic tomography results. The *P–T* conditions of crystallization were reconstructed using thermobarometry of melt inclusions. There are two key points to mention concerning the method applied to study magmatism at the Uksichan and Ichinsky Volcanoes. First, not all samples, even being fresh, contain the melt inclusions that would survive heating and quenching and ensure representative and reliable information from analysis of quenched glasses. Given that the experimental work on melt inclusions is time- and labor-consuming, the samples that potentially store fresh phenocrysts were preselected. Therefore, the melt inclusion data may come from samples which are not ideal geological and geochemical tracers of magmatism but can provide valuable evidence on physicochemical parameters of magmatic systems. The other point is that phenocrysts enclosed in volcanic rocks are a kind of samplers: they capture melts at all

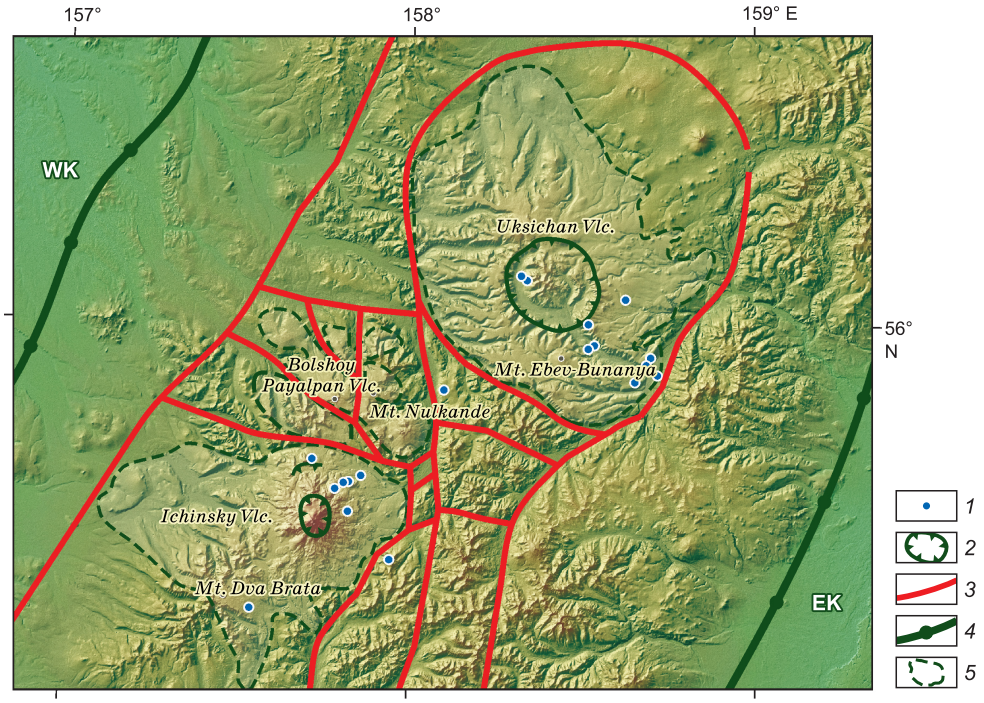

Fig. 2. Elevation map of the southwestern Sredinnyi Ridge and sampled volcanic centers. *1*, sites of detailed studies and sampling; *2*, caldera, *3*, faults, *4*, boundaries of structural units; *5*, boundaries of volcanic edifices. Abbreviations are as in Fig. 1.

depths, from the deepest to shallowest reservoirs, and thus record faithfully the evolution of magmatic systems. Note that the melt inclusion compositions are commonly characterized by no more than twenty analyses, because the inclusions have to be heated and homogenized at 1100–1200 °C and then the micrometer quenched glass they enclose have to be preconditioned and analyzed.

The compositions of minerals, specifically amphiboles from lavas, are likewise well informative as to the *P–T* conditions of magmatic systems, according to published results and our own experience (Dobretsov et al., 2016). The analytical yield on minerals is much larger than on homogenized melt inclusions, as no special experiments are needed. The Uksichan and Ichinsky lava samples that contained melt inclusions and amphibole, as well as clinopyroxene, were given most of attention because they are the best representatives of the magmatic systems. We do not claim to have modeled comprehensively the evolution of magmatism for the two volcanoes, but the physicochemical parameters of the volcanic systems retrieved from the data on melt inclusions and minerals are quite reliable and hardly possible to obtain otherwise.

The samples used to investigate the conditions of magmatism at Uksichan and Ichinsky were selected to provide representative information from melt inclusions and indicator minerals, such as amphibole. Namely, they were Uksichan basalts (K-15-16, Fig. 3) sampled by Perepelov (2014, Fig. 2.10 therein) and Davydova (2014, Figs. 2.1 and 2.2 therein) from the Middle Pliocene edifice at the base of the Uksichan volcanic center.

METHODS

The lava samples from the Uksichan and Ichinsky Volcanoes were first examined in thin sections for petrograpgy and mineralogy. The chemistry of minerals and melt inclusions was analyzed at the Analytical Center for Multi-Element and Isotope Studies and at the V.S. Sobolev Institute of Geology and Mineralogy (both in Novosibirsk). Major-element compositions were determined by XRF on a Thermo Scientific *ARL 9900 IntelliPower™ Series ARL 9900* X-ray WorkStation. The new analytical results were complemented by data recorded in the GEOROC database (http://georoc.mpch-mainz.gwdg.de/georoc/) and published by Davydova (2014).

Phenocrysts from the Uksichan and Ichinsky lavas were analyzed by EMPA on a *Camebax-Micro* electron microprobe analyzer at the V.S. Sobolev Institute of Geology and Mineralogy (Novosibirsk), while the data on groundmass microcrysts were borrowed from available publications. The detection limits of major oxides were 0.007 wt.% for SiO_2, 0.032 wt.% for TiO_2, 0.011 wt.% for Al_2O_3, 0.019 wt.% for FeO, 0.034 wt.% for MnO, 0.011 wt.% for MgO, 0.008 wt.% for CaO, 0.017 for Na_2O, and 0.009 for K_2O. The EMPA results were checked against element contents in standard samples of orthoclase (Or), diopside (Di), and garnet (O-145). The published data for Uksichan (Davydova, 2014) and Ichinsky (Dobretsov et al., 2016) volcanoes were used additionally.

Melt inclusions were studied at the Laboratory of Geodynamics and Magmatism, in the V.S. Sobolev Institute of

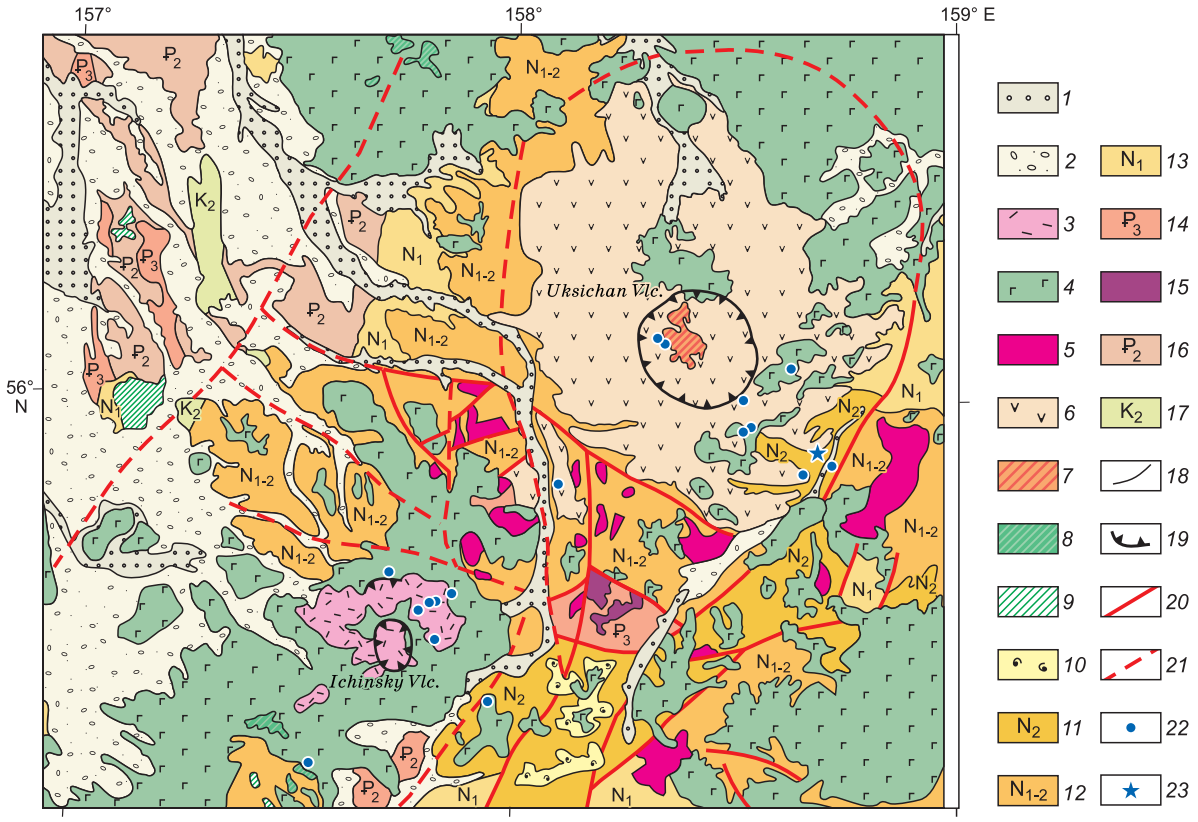

Fig. 3. Simplified geology of the southwestern Sredinnyi Ridge. *1*, Quaternary alluvium; *2*, Quaternary fluvioglacial deposits; *3*, Ichinsky Upper Pleistocene–Holocene rhyodacite and dacite lavas; *4*, Pliocene–Holocene basalt and basaltic andesite (lava flows); *5*, Pliocene–Holocene subvolcanic dacite and dacitic andesite; *6*, Pliocene–Pleistocene volcanic rocks (andesite, basaltic andesite, basalt, trachyandesite, trachybasaltic andesite); *7*, Uksichan intracaldera complex (basaltic andesite, trachydacite); *8*, Quaternary subvolcanic andesite and basalt; *9*, Pliocene–Miocene subvolcanic basalt; *10*, Pliocene–Early Pleistocene ignimbrite and rhyodacite; *11*, Pliocene volcanics (mainly intermediate lavas); *12*, Miocene and Pliocene volcanic and subvolcanic rocks (mainly intermediate and mafic lavas); *13*, Miocene sediments and volcanics (sandstone, tuffaceous sandstone, siltstone, andesitic and basaltic lavas and tuffs); *14*, Oligocene sediments (tuffaceous siltstone, tuffaceous sandstone, sandstone, conglomerate, gravelstone, and tuff); *15*, Oligocene quartz diorite and granodiorite; *16*, Eocene sediments (siltstone, sandstone, conglomerate, coal); *17*, silicic and tuffaceous silicic rocks, basalt, andesite; *18*, geological boundaries of different ages; *19*, calderas; *20*, faults; *21*, faults buried under younger rocks; *22*, sampling sites; *23*, sampling site of K-15-16 basalt. Compiled with reference to data from (Ogorodov et al., 1972; Fedotov and Mansurenkov, 1991; Perepelov, 2014).

Geology and Mineralogy (Novosibirsk). Heating-quenching experiments were run on a temperature-controlled microscope stage using inert gas (Sobolev and Slutsky, 1984) following the existing techniques (Simonov, 1993; Sobolev and Danyushevsky, 1994). The fully molten, homogenized, and quenched melt inclusions almost always consisted of homogeneous silica glass and a gas phase (gas bubble). The glass which filled the whole volume of the inclusions (except the bubble) and corresponded to the composition of the primary melts was analyzed by scanning electron microscopy. Analysis of micrometer phases in nonheated inclusions is of purely theoretical interest: their compositions are hardly suitable for retrieving physicochemical parameters while the quenched glass bears direct evidence of the melt properties. We used only experimentally heated and homogenized primary melt inclusions that record the composition of real growth media of the minerals, whereas naturally quenched melt inclusions require special calculations to reveal possible parameters of the precursor melts.

Glasses from heated melt inclusions and their host phenocrysts (clinopyroxene, orthopyroxene, plagioclase, and some amphiboles) were analyzed at the V.S. Sobolev Institute of Geology and Mineralogy (Novosibirsk) on a Tescan *MIRA 3 LMU* scanning electron microscope with an Oxford *Inca Energy 450+ XMax-80* microanalyzer. The operation conditions were: 20 keV beam energy, 1.5 nA beam current, and 20 s spectrum acquisition live time. The errors were within 1 rel.% for major elements (C > 10–15 wt.%) and from 2 to 6 rel.% (no higher than 10 rel.%) for trace elements (C = 1–10 wt.%), and up to 20 rel.% for elements approaching the detection limit of 0.2–0.3 wt.% (Lavrentiev et al., 2015).

The analytical data were processed in several successive steps in order to estimate the physicochemical parameters of melts during crystallization of the phenocrysts. First, homogenization temperatures were determined which most often corresponded to the uptake (crystallization) temperatures. The compositions of glasses in the quenched inclu-

sions were analyzed at the next step. The obtained evidence on the melt composition and the crystallization temperatures of certain minerals was used to reconstruct the respective liquidus crystallization pressure with the *Petrolog* software (Danyushevsky and Plechov, 2011). The program processes the input compositions of glasses obtained from homogenized melt inclusions and puts out pressures at which the predicted liquidus crystallization temperatures fit the best the experimental homogenization temperatures of the melt inclusions. Thus, the experimental data on melt inclusions have implications for the temperature, pressure, and melt compositions of magmatic systems at the time when phenocrysts began to crystallize.

On the other hand, zonation in phenocrysts records a complex history with variable pressures and temperatures, which can be deciphered using mineral thermometers and barometers. That was specifically the case of Uksichan samples (Davydova, 2014) analyzed by the thermobarometric method of Putirka (2008). In the reported study, several clinopyroxene and amphibole thermometers and barometers were used (Johnson and Rutherford, 1989; Mercier, 1980; Nimis and Taylor, 2000; Perchuk, 1980; Putirka et al., 1996; Schmidt, 1992; Ridolfi and Renzulli, 2012; Yavuz, 2007). Note that all results of clinopyroxene thermobarometry require checking against *P–T* parameters inferred from melt inclusion data. The consideration below includes only thus verified data.

Pressures and temperatures at the final stage of magmatism were estimated using amphibole barometers (Johnson and Rutherford, 1989; Schmidt, 1992; Yavuz, 2007) and thermometers (Ridolfi and Renzulli, 2012), of which many were tested previously (Dobretsov et al., 2016, 2017b).

Generally, we have performed comprehensive thermobarometry of samples, with multiple independent checks against (i) analyses of melt inclusions in minerals; (ii) several clinopyroxene and amphibole thermometers and barometers; (iii) experimental thermometry of melt inclusions; (iv) *P–T* parameters derived from melt inclusions and analyses of minerals with predictions by modeling in *Petrolog* (Danyushevsky and Plechov, 2011) and *Pluton* (Lavrenchuk, 2004); (v) the respective published data, and (vi) seismic tomography.

In addition, reference was made to known crystallization conditions estimated for the Uksichan lavas (Davydova, 2014) by *Comagmat* modeling (Ariskin et al., 1993; Ariskin and Barmina, 2000; Kimura and Ariskin, 2014) and by Putirka's (2008) thermometry and barometry.

SOUTHERN PART OF THE SREDINNYI RIDGE VOLCANIC BELT

The study area is shown in three figures: a generalized map of suprasubduction magmatism in Kamchatka (Fig. 1), the Uksichan and Ichinsky volcanic centers in the elevation model of the southwestern Sredinnyi Ridge (Fig. 2), and simplified geology of the Sredinnyi Ridge volcanic belt (Fig. 3). The belt consists of two almost equal parts. The southwestern part is broader than the northeastern one and accommodates large Pliocene volcanic edifices of Ichinsky and Uksichan discussed below, as well as Ketepana and Alnei–Chashakondzha.

Late Pliocene–Holocene basaltic volcanoes and cones are scattered over the southwestern belt segment and cluster in a large field of ten local centers northeast of Uksichan. In the northeastern segment, Quaternary volcanoes (Q_3–Q_4) make up a 250 km long and 20–30 km wide continuous chain extending from Alnei–Chashakondzha to Khuvkhoitun and on northward, among predominant Miocene–Oligocene volcanic complexes. The older volcanoes (attributed sometimes to the Alnei group) are exposed only in fragments, mainly south of the Ichinsky Volcano and southeast of Uksichan.

The southwestern Sredinnyi Ridge is superposed over a collisional zone with granite-gneiss domes on the extension of the volcanic belt (Fig. 1). The northernmost dome accommodates a dacitic caldera of the Khangar Volcano in the center. The southeastern part of the volcanic belt lacks basement gneisses but contains numerous small diorite intrusions (plagiogranites similar to those of granite-gneiss domes) and gneiss xenoliths at the Uksichan site (Davydova, 2014).

Uksichan V**olcano** is among largest edifices in Kamchatka: second after Shiveluch in the eruption volume and notably larger than Alnei–Chashakondzha and Ichinsky (Table 1). It is a complex multistage structure with a heavily eroded base, a younger intracaldera dacitic dome, and Quaternary basaltic volcanoes which fully cover Pliocene lavas in the north.

The history of Uksichan was previously divided into three major events (Ogorodov et al., 1972), which produced (1) the base of the volcano in the Miocene–Pliocene (volcaniclastic and pyroclastic rocks), (2) a stratovolcano composed of basalt, andesite, or less often trachynadesite and trachyte, and (3) a dacite extrusion and postcaldera alkali basalts. Stefanov and Shirokii (1980) distinguished four stages, with formation of (1) Pliocene andesite, dacite, ignimbrite, and moderately felsic tuff base of the volcano, (2) a stratovolcano composed of basaltic andesite, pumice tuff, and ignimbrite, (3) a Quaternary shield edifice and several Middle–Late Pleistocene peripheral domes of more alkaline trachydacite and trachyrhyolite, (4) Pleistocene–Holocene basaltic lava and scoria cones. The caldera originated at stage 2 and underwent differentiated subsidence at stage 3. According to recent data (Perepelov et al., 2006; Davydova, 2014; Perepelov, 2014), the formation of the Uksichan base was followed by four stages of volcanism corresponding to (1) a stratovolcano, (2) a shield volcano, (3) a caldera, and (4) postcaldera andesite-basaltic andesite shield volcanoes with proper names (Chingeingein, Ebev-Bunanya, etc.) and scoria cones with flows of subalkaline basalt or less often basaltic andesite.

The available isotope dates bracket the volcanism between 3.28 and 3.60 Ma (Middle Pliocene), including a K–Ar

Table 1. Large volcanoes of Sredinnyi Ridge (1–3) and Klyuchevskoy group (4), Kamchatka

Volcano (depth below sea level, m)		Edifice type	Size of edifice base, km	Relative elevation, m	Area, km^2	Age index	Volume of eruption, km^3				Magma Series	Predominant lithology
							Total	Mafic	Intermediate	Felsic		
1	Uksichan (1685)	Shield volcano with caldera	51 × 54	700	1850	N_2–Q_3–Q_4	750	620 (83%)	110 (15%)	20 (2%)	Basaltic dacite	Basaltic andesite
2	Alnei–Chashakondzha (2581)	Lava cone	27 × 30	1800	800	N_2–Q_4	600	490 (82%)	90 (15%)	20 (3%)	Basalt	Basalt
3	Ichinsky (3621)	Cone-shaped stratovolcano	25 × 30	2800	560	Q_3–Q_4	450	300 (67%)	80 (18%)	70 (15%)	Rhyolite-dacite-basalt	Basaltic andesite
4	Shiveluch (3283)	Andesitic lava cone	30 × 45	2900	2900	Q_3–Q_4	1100	200 (18%)	900 (82%)	0	Andesite	Andesite

Note. Table is based on published data (Kozhemyaka, 1995, 2001; Davydova, 2014).

age of 3.6 Ma (Perepelov et al., 2006), Ar–Ar ages of 3.56 ± 0.05 and 3.34 ± 0.07 Ma (Bindeman et al., 2010), and a U–Pb age of 3.28 ± 0.04 Ma (Kostitsyn and Anosova, 2013).

Ichinsky is one of two active volcanoes in the Sredinnyi Ridge (Melekestsev et al., 2001; Perepelov, 2014) composed of basalt, andesite, and rhyolite dacite alternated intricately in space and time, as well as domes and dikes highly diverse in structure and composition.

The late Holocene stage of activity (Pevzner, 2004) produced coarse volcanic sand and unsorted pyroclastics consisting of typical island-arc moderately magnesian calc-alkaline andesite and dacite. In the Holocene, the Ichinsky Volcano erupted in Early and Late Holocene, with a 2500 yr long lull. The early Holocene event began with several medium eruptions (mainly tephra), peaked about 6500 yr BP having produced voluminous pyroclastics found in sections of the respective ages, and ended with large andesite-dacite extrusion. The late Holocene event began about 4200 yr ago and comprised several eruptions recorded in pyrclastic flows. The latest known eruption produced a thick dacite lava flow on the southwestern slope of the volcano in 1740.

The Ichinsky volcanic history consists of several stages reconstructed with reference to the model of Kutyev (1975): (1) olivine basalt domes with craters up to 200 m in diameter at the base of the volcano; (2) flows of subalkaline basalt and basaltic andesite in the northern part of the volcano; (3) amphibole dacite and rhyodacite composite domes, including Gigilen dome in the northeastern volcano part; (4) andesite (grading into basaltic and dacitic andesite) in the main part of the cone, partly ice-capped; (5) dacite flows, up to 5–6 km long, beginning with rhyodacite domes on a fragmentary caldera; (6) W–E and radiated felsic dikes.

MAJOR-ELEMENT COMPOSITIONS

The major-element compositions of the Uksichan and Ichinsky lavas characterized by new and published data

Table 2. Representative analyses of Uksichan and Ichinsky lava samples, this study (wt.%)

No.	Sample	Rock	SiO_2	TiO_2	Al_2O_3	Fe_2O_3	MnO	MgO	CaO	Na_2O	K_2O	P_2O_5	LOI	Total
1	U-1	Basaltic andesite	56.15	1.00	17.80	8.10	0.15	2.19	6.34	3.80	3.12	0.51	0.22	99.37
2	U-2	Andesite	57.11	0.99	17.32	7.98	0.17	2.19	6.22	3.72	3.11	0.52	0.17	99.49
3	U-3	Basaltic andesite	56.23	1.02	17.61	8.08	0.20	1.94	6.02	3.72	3.17	0.52	0.56	99.08
4	U-4	Basaltic andesite	55.34	1.02	17.88	8.12	0.15	2.65	6.64	3.62	3.05	0.50	0.16	99.14
5	U-5	Basaltic andesite	56.21	1.00	18.06	8.01	0.14	2.31	6.34	3.77	3.13	0.50	0.26	99.73
6	K-15-16	Basalt	52.65	0.86	18.27	9.78	0.16	4.96	8.71	3.12	0.69	0.16	0.33	99.71
7	K-20-16	Dacite	68.81	0.49	14.78	3.47	0.10	1.28	2.95	4.53	2.08	0.10	0.66	99.26
8	K-2B-16	Dacite	65.12	0.55	15.69	4.12	0.09	1.55	3.49	4.22	3.02	0.17	0.89	98.92
9	K-3A-16	Dacite	65.43	0.53	15.64	4.06	0.08	2.17	3.49	4.19	2.90	0.18	0.22	98.89
10	1405	Andesite	59.91	0.64	16.66	6.00	0.13	2.44	5.15	3.88	2.49	0.28	1.53	99.10
11	1402	Dacite	66.23	0.57	16.13	4.42	0.09	1.56	3.65	4.10	3.00	0.19	0.12	100.06
12	1401	Basalt	51.23	1.98	16.18	12.03	0.17	4.26	7.39	3.59	2.48	0.72	–0.72	99.32
13	1403	Andesite	62.92	0.66	16.69	5.52	0.10	2.36	4.94	3.84	2.42	0.22	0.10	99.75
14	6A(1402)	Andesite	66.61	0.52	15.81	4.07	0.08	1.49	3.38	4.11	3.12	0.17	0.27	99.62

Note. 1–7 are Uksichan samples; 8–14, are Ichinsky samples.

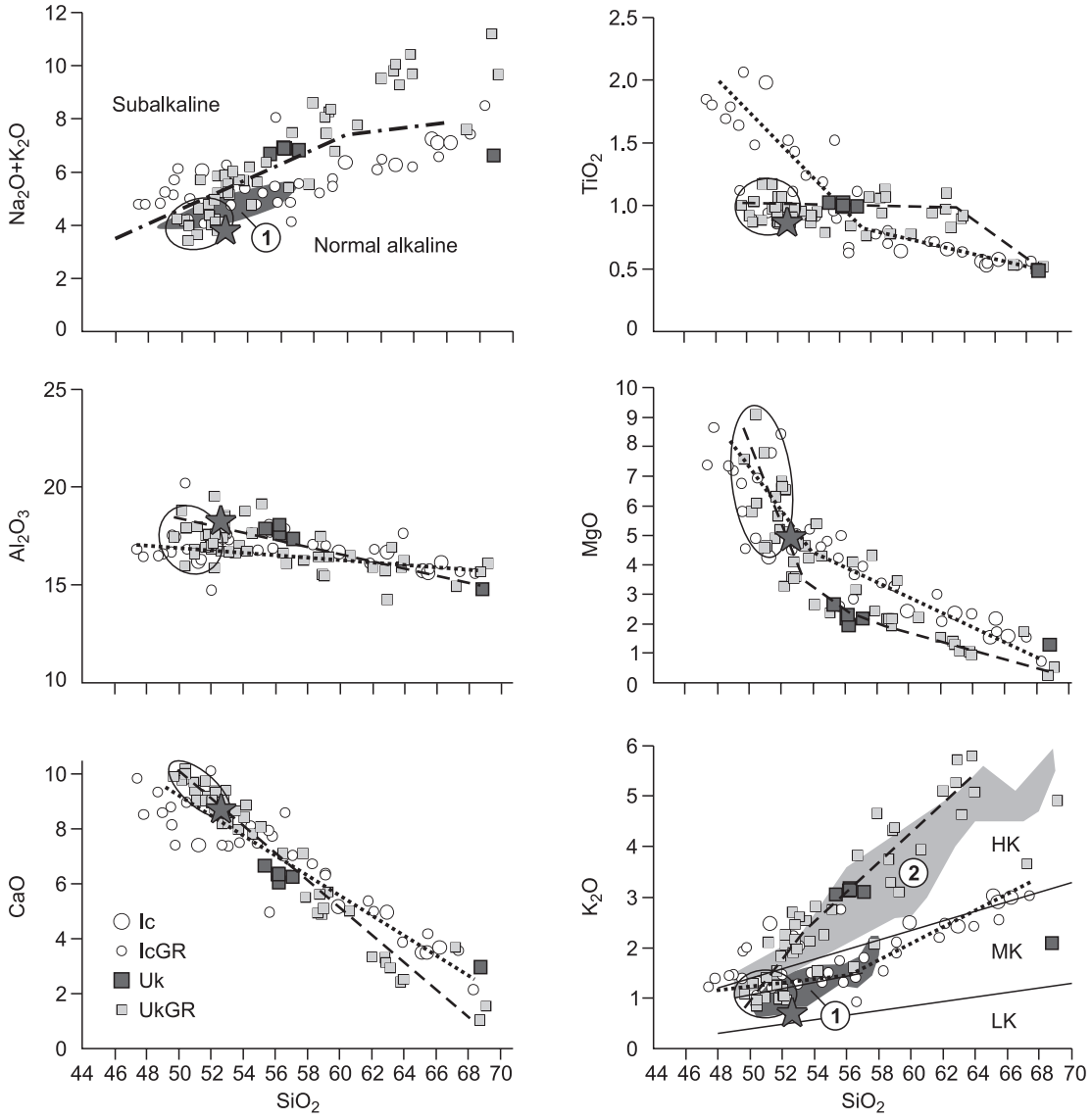

Fig. 4. Major-element compositions (wt.%) of Uksichan and Ichinsky samples. The data include original results by the authors for Ichinsky and the Uksichan Volcanoes (Ic and Uk, respectively); analyses of Ichinsky and Uksichan lavas from GEOROC database (http://georoc.mpch-mainz.gwdg.de/georoc/) (IcGR and UkGR, respectively) and data from Davydova (2014). Solid line contours the Uksichan moderately potassic basalt compositions based on GEOROC database (http://georoc.mpch-mainz.gwdg.de/georoc/) and data from Davydova (2014). Asterisk denotes basalt sample K-15-16 from the Uksichan Volcano. 1 and 2 are fields of Uksichan basalt and basaltic andesite from stratovolcano and shield volcano with moderate (Davydova, 2014) and high (Antipin et al., 1987; Perepelov, 2014) potassium contents, respectively. LK, low-K series; MK, moderately K series; HK, high-K series, according (Bogatikov et al., 2009). Chain line separates subalkaline and alkaline compositions; dash and dotted lines are composition trends of the Uksichan and Ichinsky Volcanoes, respectively. Compiled with reference to data from (Bogatikov, 1983; Bogatikov and Kovalenko, 1987).

(Table 2) show some features of difference. Specifically, the Ichinsky basalts are subalkaline while the Uksichan tholeiitic basalts are alkaline (Fig. 4), and the Ichinsky andesites are calc-alkaline unlike the subalkaline Uksichan andesites. The titanium and potassium patterns are different as well: TiO_2 is stable and moderate (1.2 wt.%) in Uksichan but varies from higher values of 2.06 wt.% to as low as 0.5 wt.% at increasing SiO_2 in Ichinsky (see the TiO_2–SiO_2 diagram in Fig. 4); K_2O is from ≥2 wt.% (at SiO_2 = 52 wt.%) to 5.8 wt.% (at SiO_2 = 64 wt.%) in the Uksichan samples and lower in the Ichinsky rocks (3.03 wt.% at SiO_2 = 68 wt.%). The revealed moderately and highly potassic compositions of the Uksichan lavas (Fig. 4) are consistent with their assignment (Perepelov, 2014) to moderately potassic, highly potassic, and shoshonite-latite series. A basalt sample studied in detail (K-15-16) has a moderately potassic major-element composition and falls in the field of moderately potassic basalt and basaltic andesite (Fig. 4).

In general, major-element analyses show that magmatism of the two volcanoes shares similarity in composition trends

(decreasing Mg and Ca at increasing SiO_2, see Fig. 4) but differs in in total alkalis and in the contents of TiO_2 and K_2O: maximum TiO_2 in Ichinsky and maximum potassium increase at increasing SiO_2 in Uksichan.

MINERAL CHEMISTRY

Mineral chemistry was analyzed in clinopyroxene, orthopyroxene, amphibole, and plagioclase from the Uksichan and Ichinsky lavas (Tables 3–6). New data have been obtained for the compositions of orthopyroxene and amphibole in samples from both volcanoes and for clinopyroxene and plagioclase in those from Uksichan only. For more complete characterization, reference was made to our previous publication (Dobretsov et al., 2016) and to the results reported by Davydova (2014).

The Uksichan basalt samples contain **clinopyroxene** (phenocrysts and groundmass microcrysts) with augite compositions and bronsite to hypersthene **orthopyroxene** (phenocrysts and microcrysts) according to the shares of the En–Wo–Fs components (Fig. 5); some orthopyroxene microcrysts, with greater Wo enrichment, belong to Mg pigeonite. Most of the clino- and orthopyroxene compositions plot between the 1100 and 1200 °C isotherms (Fig. 5).

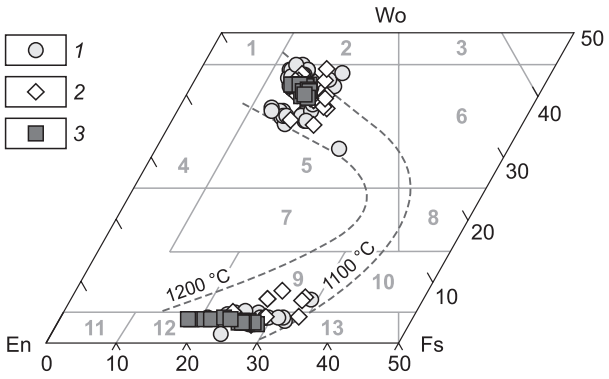

Fig. 5. Compositions of pyroxenes from Uksichan basalt samples. *1*, *3*, pyroxene phenocrysts from basalt, after (Davydova, 2014) (*1*) and this study (*3*); *2*, pyroxene from basalt groundmass, after (Davydova, 2014). Isotherms are after (Davydova, 2014). Numerals in the diagram are composition fields of pyroxenes (Godovikov, 1975): 1, diopside, 2, salite, 3, ferrosalite, 4, endiopside, 5, augite, 6, ferroaugite, 7, subcalcic augite, 8, subcalcic ferroaugite, 9, magnesian pigeonite, 10, intermediate pigeonite, 11, enstatite, 12, bronsite, 13, hypersthene.

Orthopyroxene and clinopyroxene show marked variations in the AI^{IV}–Ca and Mg#–Ca diagrams (Fig. 6). The phenocrystic and microcrystic pyroxenes contain compa-

Table 3. Representative analyses of clinopyroxene from Uksichan lavas (wt.%), this study

No.	Analysis number and place	SiO_2	TiO_2	Al_2O_3	Cr_2O_3	FeO	MnO	MgO	CaO	Na_2O	K_2O	Total	Mg#
1	51 r	51.41	0.44	2.93	0.18	8.66	0.24	15.40	19.99	0.27	0.01	99.53	76.01
2	52 int	51.59	0.52	2.67	0.02	9.09	0.38	14.98	20.00	0.30	0.00	99.56	74.60
3	53 int	51.59	0.49	2.47	0.00	9.06	0.37	15.18	19.86	0.28	0.00	99.30	74.91
4	54 int	51.74	0.47	2.36	0.00	8.91	0.34	15.25	20.04	0.29	0.00	99.40	75.31
5	55 c	51.88	0.47	2.34	0.00	9.02	0.34	15.19	20.03	0.30	0.00	99.56	75.01
6	56 r	51.10	0.52	2.08	0.01	10.34	0.34	15.12	19.30	0.30	0.00	99.11	72.27
7	57 int	51.99	0.50	1.95	0.00	10.12	0.35	14.72	19.54	0.31	0.00	99.47	72.16
8	58 int	51.51	0.52	2.01	0.04	9.73	0.35	14.59	19.59	0.32	0.00	98.67	72.77
9	59 int	51.39	0.54	2.10	0.02	10.12	0.38	14.66	19.72	0.30	0.00	99.23	72.08
10	60 c	51.10	0.55	2.03	0.00	9.94	0.38	14.69	20.14	0.36	0.00	99.18	72.48
11	61 r	52.64	0.46	1.67	0.04	9.66	0.39	15.30	19.88	0.34	0.00	100.38	73.84
12	62 int	52.38	0.47	1.79	0.00	9.43	0.44	14.83	19.89	0.32	0.00	99.55	73.70
13	63 int	51.99	0.47	1.73	0.00	9.64	0.43	14.87	19.86	0.33	0.00	99.32	73.32
14	64 int	51.82	0.48	1.70	0.00	9.57	0.42	14.85	19.90	0.32	0.00	99.06	73.44
15	65 int	52.22	0.43	1.57	0.02	9.55	0.40	14.93	19.88	0.29	0.00	99.29	73.59
16	66 c	51.85	0.49	1.86	0.02	9.67	0.39	14.87	19.86	0.29	0.00	99.31	73.26
17	67 r	51.39	0.46	2.85	0.14	8.27	0.19	15.23	19.64	0.24	0.00	98.41	76.64
18	68 int	51.83	0.48	1.76	0.03	9.59	0.36	15.22	18.98	0.31	0.00	98.56	73.88
19	69 int	52.32	0.43	2.09	0.04	9.12	0.32	14.99	19.88	0.29	0.00	99.48	74.55
20	70 c	51.31	0.48	1.72	0.02	9.68	0.35	14.98	19.26	0.31	0.00	98.11	73.39
21	71 c	51.17	0.50	1.94	0.02	10.09	0.33	14.98	19.73	0.31	0.00	99.07	72.57
22	72 int	51.05	0.51	2.02	0.01	10.30	0.32	14.93	19.62	0.35	0.01	99.12	72.09
23	73 int	51.24	0.50	2.08	0.02	10.54	0.32	15.17	19.12	0.33	0.00	99.33	71.95
24	74 r	51.48	0.50	2.48	0.01	9.95	0.29	15.00	19.01	0.31	0.01	99.03	72.87

Note. Clinopyroxene phenocrysts from Uksichan (sample K-15-16). Hereafter: abbreviations stand for place of analysis: c, core; int, intermediate; r, rim. Mg# = Mg·100/(Mg + Fe), apfu.

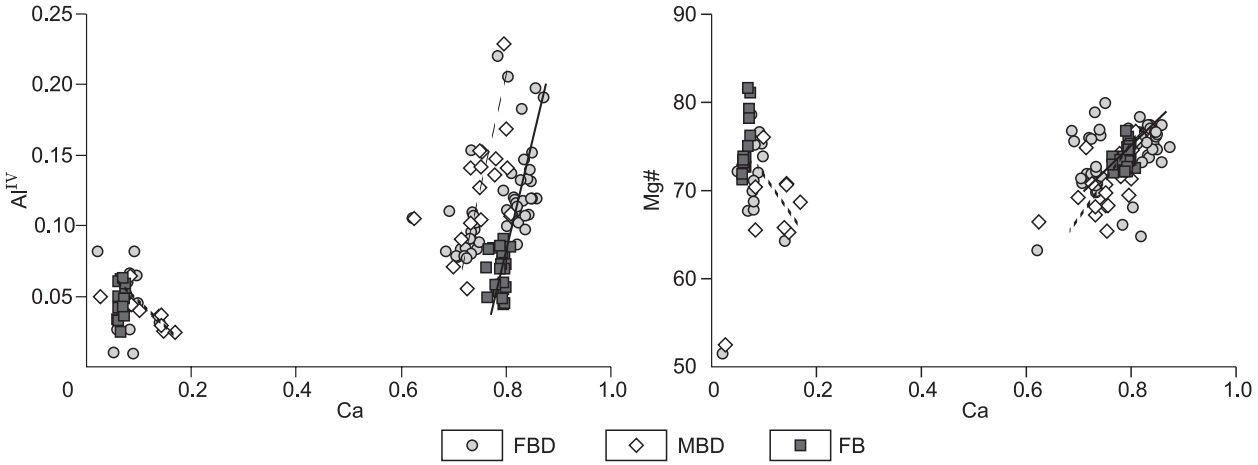

Fig. 6. Al^{IV}–Ca and Mg#–Ca diagrams (apfu) for pyroxenes from the Uksichan basalt samples. PBD and MBD, basalt varieties according to Davydova (2014): phenocrysts (FBD) and groundmass microcrysts (MBD); PB, phenocrysts from basalt, this study. Solid and dash lines are pyroxene composition trends for phenocrysts and microcrysts, respectively. Mg# = Mg·100/(Mg + Fe), apfu.

rable element concentrations. As Ca increases, the contents of Al and Mg# increase in clinopyroxene, in accordance with the whole rock trends (Fig. 4), but decrease from phenocrysts to microcrysts in orthopyroxene (Fig. 6).

The chemistry of **olivine** in the Uksichan samples changes as a function of crystallization conditions. In the MnO–Fo and CaO–Fo diagrams, manganese and calcium increase as Fo decreases in the series phenocryst core–phenocryst rim–microcryst (Fig. 7). The cores of phenocrysts are the most magnesian and split into two groups: Fo = 82–76 apfu and Fo = 75–60 apfu. Forsterite is lower in the rims of phenocrysts (mainly Fo = 67–61 apfu) and minimum (52 apfu) in microcrysts. All olivines likewise form two groups with different contents of Mn and Ca but with the same trend of Fo decrease from phenocryst cores to microcrysts (Fig. 7). Thus the olivine compositions record changes in the conditions of crystallization from phenocrysts to microcrysts.

Amphibole was studied in the Uksichan dacite and latite, and in the Ichinsky dacite and andesite samples. The dacitic amphibole from both volcanoes has a Mg-hornblendite composition and corresponds to varieties from calc-alkaline rocks, while that from andesite and latite is of Mg-hastingsite composition and likewise falls in the calc-alkaline field (Fig. 8). The K_2O–Al^{VI} patterns in amphibole differ between the samples of the two volcanoes: relatively high Al^{VI} at almost invariable K_2O at Ichinsly and concurrent Al^{VI} and K_2O increase at Uksichan (Fig. 8).

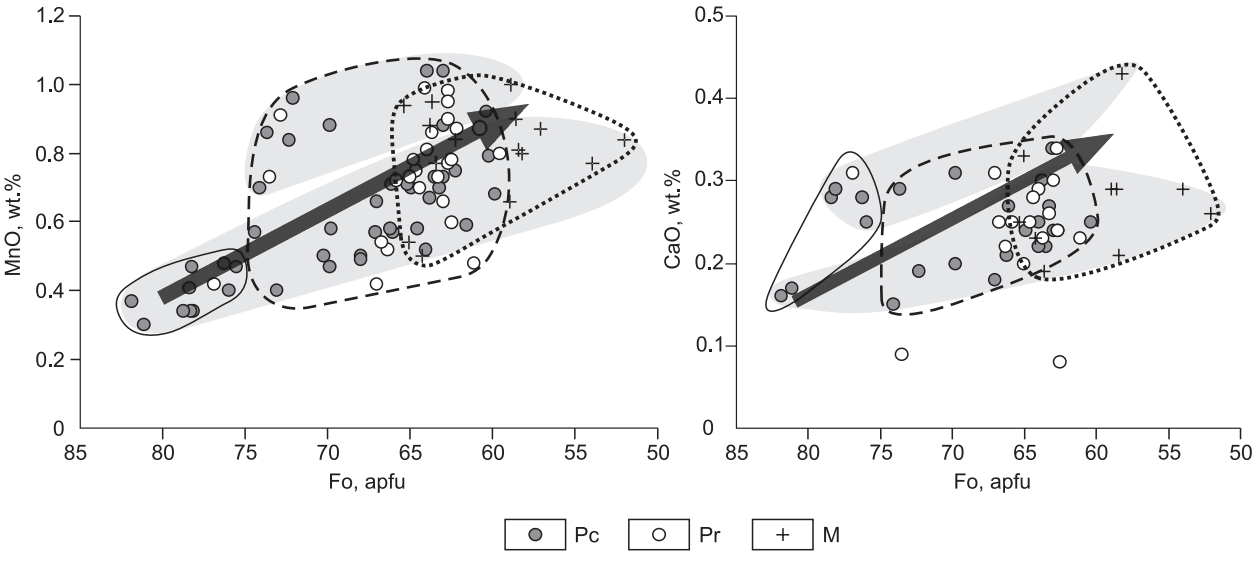

Fig. 7. MnO–Fo and CaO–Fo diagrams for olivine from the Uksichan samples. Pc, Pr, M stand for phenocryst (core), phenocryst (rim) and microcryst, respectively, according to (Davydova, 2014). Solid, dash, and dotted lines contour, respectively, primitive (early) group, late phases, and microcrysts. Gray color shows groups of olivines according to Mn and Ca contents. Arrows show average trends of olivine compositions at decreasing Fo.

Table 4. Representative analyses of orthopyroxenes from Uksichan and Ichinsky lavas (wt.%), this study

No.	Analysis number and place	SiO_2	TiO_2	Al_2O_3	Cr_2O_3	FeO	MnO	MgO	CaO	Na_2O	K_2O	Total	Mg#
1	37 r	53.37	0.27	1.38	0.00	17.18	0.60	25.65	1.69	0.02	0.00	100.17	72.68
2	38 int	54.24	0.25	1.03	0.02	18.07	0.60	25.08	1.55	0.01	0.00	100.86	71.21
3	39 int	54.15	0.19	0.86	0.02	17.24	0.65	25.89	1.64	0.03	0.00	100.67	72.80
4	40 int	54.58	0.18	0.76	0.03	16.52	0.64	25.94	1.71	0.02	0.00	100.38	73.67
5	41 c	53.93	0.24	1.15	0.01	17.67	0.66	25.25	1.55	0.02	0.00	100.48	71.80
6	42 r	54.11	0.22	1.31	0.00	16.28	0.49	25.76	1.60	0.04	0.00	99.81	73.82
7	43 c	53.84	0.22	1.21	0.00	16.92	0.49	25.93	1.60	0.04	0.00	100.26	73.20
8	44 r	53.46	0.22	1.45	0.00	16.77	0.50	25.99	1.56	0.02	0.00	99.97	73.42
9	45 int	54.73	0.29	1.52	0.06	12.07	0.45	28.95	1.95	0.04	0.01	100.05	81.04
10	46 c	55.05	0.23	1.31	0.04	13.10	0.50	28.05	1.89	0.04	0.00	100.22	79.23
11	47 r	54.65	0.29	1.42	0.04	13.79	0.45	27.79	1.88	0.04	0.01	100.35	78.22
12	48 int	55.11	0.24	1.02	0.04	11.77	0.63	29.30	1.87	0.02	0.00	100.01	81.60
13	49 int	53.64	0.28	1.81	0.03	14.84	0.42	26.57	1.95	0.03	0.00	99.57	76.14
14	50 int	53.83	0.28	1.81	0.04	15.71	0.41	26.46	1.82	0.03	0.00	100.39	75.01
15	85 int	54.20	0.15	0.55	0.08	19.75	1.87	23.56	0.83	0.02	0.00	101.00	68.01
16	86 int	54.74	0.10	0.38	0.10	19.07	1.88	23.47	0.73	0.01	0.00	100.46	68.68
17	87 r	54.21	0.12	0.60	0.11	18.96	1.72	23.94	0.90	0.03	0.00	100.58	69.23
18	88 c	53.42	0.13	0.80	0.02	18.95	1.81	23.72	0.67	0.02	0.00	99.54	69.05
19	111 int	53.81	0.09	0.39	0.00	20.15	1.59	23.13	0.67	0.01	0.00	99.84	67.17
20	112 int	54.03	0.11	0.41	0.01	19.13	1.22	23.55	0.91	0.01	0.00	99.37	68.69
21	113 int	53.61	0.09	0.33	0.00	21.01	1.75	22.49	0.65	0.01	0.00	99.93	65.61
22	114 int	53.54	0.08	0.35	0.04	20.73	1.78	23.15	0.63	0.03	0.01	100.33	66.56
23	115 int	54.00	0.09	0.31	0.03	20.45	1.80	22.62	0.64	0.03	0.01	99.98	66.34
24	122 r	54.19	0.09	0.30	0.02	19.09	1.18	23.98	0.80	0.03	0.00	99.68	69.12
25	123 int	53.33	0.14	0.48	0.01	20.61	1.59	23.09	0.81	0.02	0.00	100.09	66.63
26	125 c	53.63	0.08	0.28	0.01	19.01	1.19	23.60	0.74	0.00	0.00	98.53	68.87
27	126 r	53.88	0.13	0.57	0.00	19.35	1.18	23.66	0.88	0.02	0.00	99.68	68.54
28	127 c	53.74	0.11	0.59	0.03	19.49	1.20	23.85	0.85	0.03	0.00	99.90	68.56
29	128 r	53.62	0.10	0.42	0.01	20.49	1.47	23.40	0.73	0.02	0.00	100.25	67.05

Note. 1–18 are orthopyroxene phenocrysts from Uksichan basalt (1–14, sample K-15-16) and dacite (15–18, sample K-20-16); 19–29 (sample K-3A-16) are orthopyroxenes from Ichinsky dacite.

Plagioclase from the Uksichan basalt was analyzed during melt inclusion studies. Feldspar compositions (analyzed near melt inclusions) are listed in Table 6. The Uksichan plagioclase has a labradorite–bytownite composition according to the content of anorthite (60–81 An). Some information on the evolution of magmatic systems was inferred from core to rim composition variations in phenocrysts from both Uksichan and Ichinsky samples.

Clinopyroxene was studied according to growth zones only in the Uksichan basalt and three main evolution patterns were revealed in phenocrysts: (i) slight Mg# increase and TiO_2 decrease; (ii) general Mg# decrease and TiO_2 increase (reverse in the rim); (iii) distinct Mg# increase and TiO_2 decrease. The first case corresponds to quite stable crystallization conditions without any notable *PTX* fluctuations. The second case approaches the standard fractionation process in a closed chamber, with accumulation of Ti residual magma, followed by crystallization of clinopyroxene from a more magnesian melt. These features may record continuous inputs of new batches of deep magmas into connected magma reservoirs located at different depths and closure of the system leading to fractional crystallization with Mg# decrease and Ti increase (see below).

Orthopyroxene phenocrysts in the Uksichan basalt are commonly very fine and are much more altered than the clinopyroxene phenocrysts. The composition variations from core to rim are rarely detectable, but the plots for ortho- and clinopyroxenes turn out to be similar, in spite of variable Mg#. Pyroxene first grew from a melt which lost magnesium and gained titanium. At the final stage, when rims were crystallizing, Mg# increased markedly while TiO_2 decreased, as in the case of clinopyroxene, most likely due to inputs of a more primitive mantle melt.

Amphibole from Uksichan was studied mainly in dacite. Its composition varies uniformly from core to rim: Al_2O_3 grows slightly while K_2O remains almost invariable. Or, the

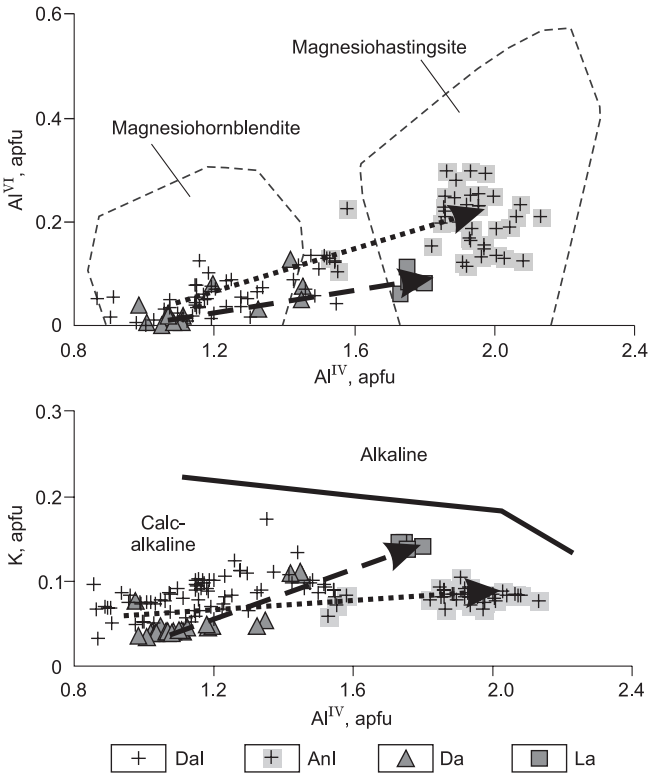

Fig. 8. Al^{VI}–Al^{IV} and K–Al^{IV} diagrams for amphibole from the Uksichan and Ichinsky samples. Abbreviations denote amphiboles from Ichinsky dacite (DaI) and andesite (AnI) and from Uksichan dacite (Da) and latite (La). Dotted and dash lines are trends for amphiboles from the Ichinsky and Uksichan lavas, respectively. Compiled using data of this study and published results (Davydova, 2014; Dobretsov et al., 2016).

components first grow, then decrease steadily, and then increase rapidly in rims at the final crystallization stage (Fig. 9).

MELT INCLUSIONS

Data on melt inclusions in minerals from the Ichinsky lavas were reported in our pervious publications (Dobretsov et al., 2016; Simonov and Kotlyarov, 2016). New results have been obtained for melt inclusions in clinopyroxene, plagioclase, and orthopyroxene from samples of Middle Pliocene stratovolcanic edifices at the base of Uksichan.

Primary melt inclusions (10–35 μm) in **clinopyroxene** (Fig. 10*A*) commonly follow growth zones. Spherical inclusions comprise several distinct light and dark phases and a fluid phase (bubble). The experiments show homogenization between 1190 and 1215 °C. The heated and quenched inclusions contain light glass and a fluid bubble (Fig. 11*A*).

Primary melt inclusions (up to 60–100 μm) in **plagioclase** are arranged uniformly parallel to the crystal faces. They often have elongate prismatic shapes and, in their turn, enclose numerous phases: clinopyroxene, plagioclase, ore microcrysts, and bubbles (Fig. 10*B*). Experiments show that inclusions in plagioclase homogenize in a larger temperature ridge of 1175 to 1240 °C and are filled with light homogeneous glass with a small bubble, like those in plagioclase (Fig. 11*B*).

Melt inclusions (to 25 μm) in **orthopyroxene** are found much more rarely than those in clinopyroxene and plagioclase. They commonly follow growth zones and contain several phases. The homogenization temperature ridge is intermediate between those for clinopyroxene and plagioclase: 1180–1225 °C.

The compositions of glasses from heated and homogenized inclusions in minerals from the Uksichan basalt (Table 7) have implications for the primary melt compositions. They show alkaline chemistry in the (Na_2O + K_2O)–SiO_2 diagram, as well as the respective basalt sample (K-15-16). Most of melt inclusions have SiO_2 contents from 47.8 to 56.8 wt.% corresponding to basalt and basaltic andesite; inclusions in clinopyroxene are high-Mg varieties (6.8–9.3 wt.% MgO).

The host basalt samples (Table 2) and the heated melt inclusions (Table 7) share similarity in K_2O contents (0.69 wt.% against 0.5–0.9 wt.%, respectively) and in total alkalis (TAS diagram). The Uksichan lavas in general are highly potassic, unlike the K-15-16 sample, in which the relatively low K_2O contents in both bulk rock and melt inclusions may be due to its location in the Middle Pliocene base beneath the later high-K lavas.

Most of the major-element patterns in variation diagrams are similar for inclusions in plagioclase and for the Uksi-

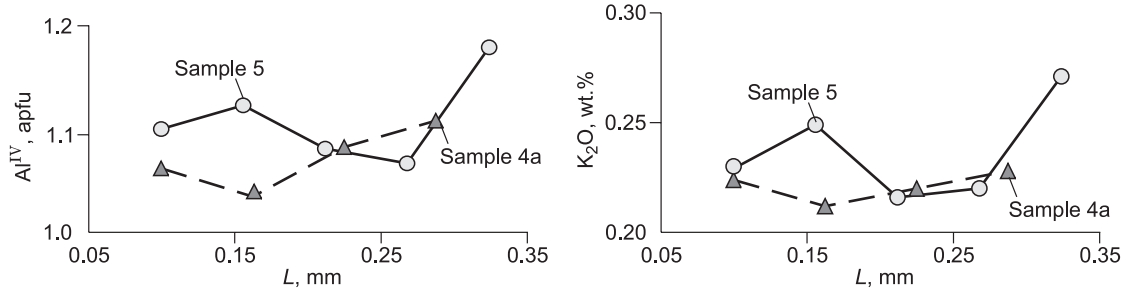

Fig. 9. Variations in Al^{IV} (apfu) and K_2O (wt.%) contents in amphibole phenocrysts from Uksichan dacite. *L* is distance from analysis point to phenocryst center.

Table 5. Representative analyses of amphiboles from Uksichan and Ichinsky lavas (wt.%), this study

No.	Analysis number and place	SiO_2	TiO_2	Al_2O_3	FeO	MnO	MgO	CaO	Na_2O	K_2O	Total	Al^{IV}
1	75 r	49.09	1.50	6.13	11.47	0.57	16.17	10.61	1.55	0.22	97.31	1.02
2	76 int	48.33	1.52	6.20	11.65	0.59	16.05	10.66	1.58	0.22	96.80	1.04
3	79 r	48.65	1.48	6.50	11.48	0.61	15.90	10.58	1.62	0.22	97.04	1.07
4	80 int	48.14	1.60	6.70	11.81	0.62	15.55	10.72	1.68	0.23	97.05	1.11
5	82 int	48.80	1.39	6.25	11.77	0.66	15.86	10.79	1.54	0.26	97.32	1.05
6	83 c	48.88	1.41	6.15	11.77	0.72	15.85	10.69	1.55	0.21	97.23	1.03
7	89 r	48.10	1.55	6.59	11.83	0.62	15.57	10.71	1.63	0.23	96.83	1.11
8	90 int	48.29	1.59	6.45	11.57	0.61	15.74	10.86	1.59	0.22	96.92	1.08
9	91 int	48.82	1.52	6.16	11.67	0.61	15.88	10.78	1.59	0.21	97.24	1.04
10	92 c	48.35	1.58	6.32	11.74	0.61	15.99	10.74	1.61	0.22	97.16	1.06
11	93 r	46.80	1.80	6.97	11.87	0.69	15.35	10.67	1.76	0.25	96.16	1.18
12	94 int	49.01	1.44	6.03	11.29	0.60	16.08	10.69	1.50	0.19	96.83	1.01
13	96 int	47.31	1.92	7.52	12.01	0.57	14.91	10.75	1.85	0.26	97.10	1.20
14	97 c	49.74	1.47	6.14	11.22	0.62	16.19	10.58	1.59	0.20	97.75	0.98
15	98 r	47.80	1.77	7.01	12.09	0.58	15.50	10.94	1.72	0.27	97.68	1.18
16	99 int	48.21	1.58	6.40	11.48	0.58	15.67	10.64	1.64	0.22	96.42	1.07
17	100 int	48.35	1.64	6.44	11.83	0.60	15.89	10.77	1.68	0.22	97.42	1.08
18	101 int	47.68	1.67	6.65	11.86	0.59	15.80	10.58	1.74	0.25	96.82	1.12
19	102 c	47.92	1.69	6.51	11.73	0.60	15.77	10.85	1.69	0.23	96.99	1.10
20	103 r	49.02	1.52	5.77	11.46	0.47	15.94	10.96	1.39	0.42	96.95	0.97
21	106 r	48.91	1.39	5.89	11.63	0.51	16.03	10.79	1.43	0.40	96.98	0.99
22	107 int	48.87	1.40	6.00	11.79	0.50	15.98	10.89	1.45	0.41	97.29	1.01
23	108 int	48.03	1.63	6.52	12.04	0.55	15.21	10.90	1.52	0.47	96.87	1.07
24	109 int	47.00	1.91	7.18	12.71	0.50	14.69	11.02	1.64	0.55	97.20	1.20
25	110 c	47.23	1.80	7.17	11.92	0.40	14.94	10.53	1.65	0.53	96.17	1.17
26	117 r	48.09	1.50	5.80	11.66	0.46	16.00	10.86	1.47	0.41	96.24	0.99
27	119 int	48.34	1.32	5.13	11.46	0.44	16.76	10.95	1.36	0.38	96.14	0.89
28	121 c	46.64	1.84	6.79	11.64	0.34	15.73	10.83	1.72	0.49	96.02	1.16
29	129 r	48.56	1.33	5.59	11.45	0.55	15.67	10.65	1.33	0.40	95.54	0.95
30	130 int	49.39	1.28	5.28	11.55	0.56	15.93	10.82	1.24	0.37	96.42	0.89
31	131 int	45.99	2.01	7.83	13.22	0.53	14.04	10.89	1.80	0.59	96.89	1.29
32	132 int	48.05	1.65	6.69	12.39	0.54	15.22	10.78	1.57	0.44	97.32	1.11
33	133 int	47.27	1.86	6.93	12.27	0.49	14.85	10.70	1.63	0.48	96.49	1.15
34	134 c	47.19	1.99	7.22	12.36	0.50	14.74	10.67	1.69	0.50	96.85	1.18
35	142 r	49.41	1.35	5.42	11.03	0.54	16.10	10.59	1.39	0.37	96.21	0.90
36	143 int	46.08	2.27	7.74	11.88	0.39	14.70	11.00	1.89	0.61	96.56	1.28
37	144 c	46.54	2.15	7.41	11.54	0.34	15.14	10.92	1.81	0.57	96.42	1.23
38	145 int	46.89	1.99	7.16	11.20	0.39	15.24	10.87	1.76	0.54	96.04	1.17
39	146 int	47.80	1.68	6.55	11.16	0.47	15.54	10.75	1.59	0.47	96.01	1.07
40	147 r	49.61	1.32	5.40	10.87	0.55	15.98	10.57	1.37	0.36	96.03	0.86
41	148 r	47.99	1.74	6.61	11.25	0.43	15.77	10.79	1.59	0.50	96.67	1.10
42	149 int	46.18	2.21	7.66	11.94	0.41	14.82	10.88	1.84	0.61	96.54	1.28
43	150 int	47.19	1.85	7.18	11.39	0.40	15.19	10.81	1.76	0.52	96.29	1.15
44	152 c	44.53	2.42	8.97	12.23	0.41	13.92	10.70	2.06	0.72	95.95	1.44
45	153 r	48.24	1.65	6.11	11.18	0.47	16.36	10.51	1.67	0.41	96.60	1.03
46	154 int	45.20	2.36	8.28	12.18	0.43	15.04	10.60	2.08	0.58	96.75	1.41
47	155 int	45.64	2.34	8.05	12.53	0.53	14.90	10.69	2.08	0.60	97.36	1.37
48	156 int	48.04	1.53	6.06	11.58	0.64	16.48	10.41	1.62	0.41	96.77	1.02
49	157 c	47.95	1.60	6.22	11.22	0.47	16.57	10.49	1.69	0.43	96.64	1.05
50	160 r	45.69	2.18	8.20	12.18	0.45	14.47	10.83	1.99	0.48	96.47	1.34
51	161 int	48.02	1.66	6.39	11.17	0.44	15.70	10.76	1.60	0.42	96.16	1.06
52	162 int	44.71	2.64	8.89	11.94	0.35	14.36	10.90	2.13	0.49	96.41	1.46
53	164 c	44.24	2.50	8.89	12.57	0.43	13.95	10.74	2.16	0.54	96.02	1.49
54	166 r	47.14	1.94	7.03	11.78	0.50	14.97	10.90	1.77	0.51	96.54	1.15
55	167 c	47.11	1.89	7.06	11.69	0.50	15.34	10.88	1.80	0.55	96.82	1.19

Note. 1–20 are amphibole phenocrysts from Uksichan dacite (sample K-20-16); 21–55 are amphiboles from Ichinsky dacite (21–34 are for sample K-3A-16; 35–55 are for sample K-2C-16). Al^{IV} is four-fold coordinated Al, apfu.

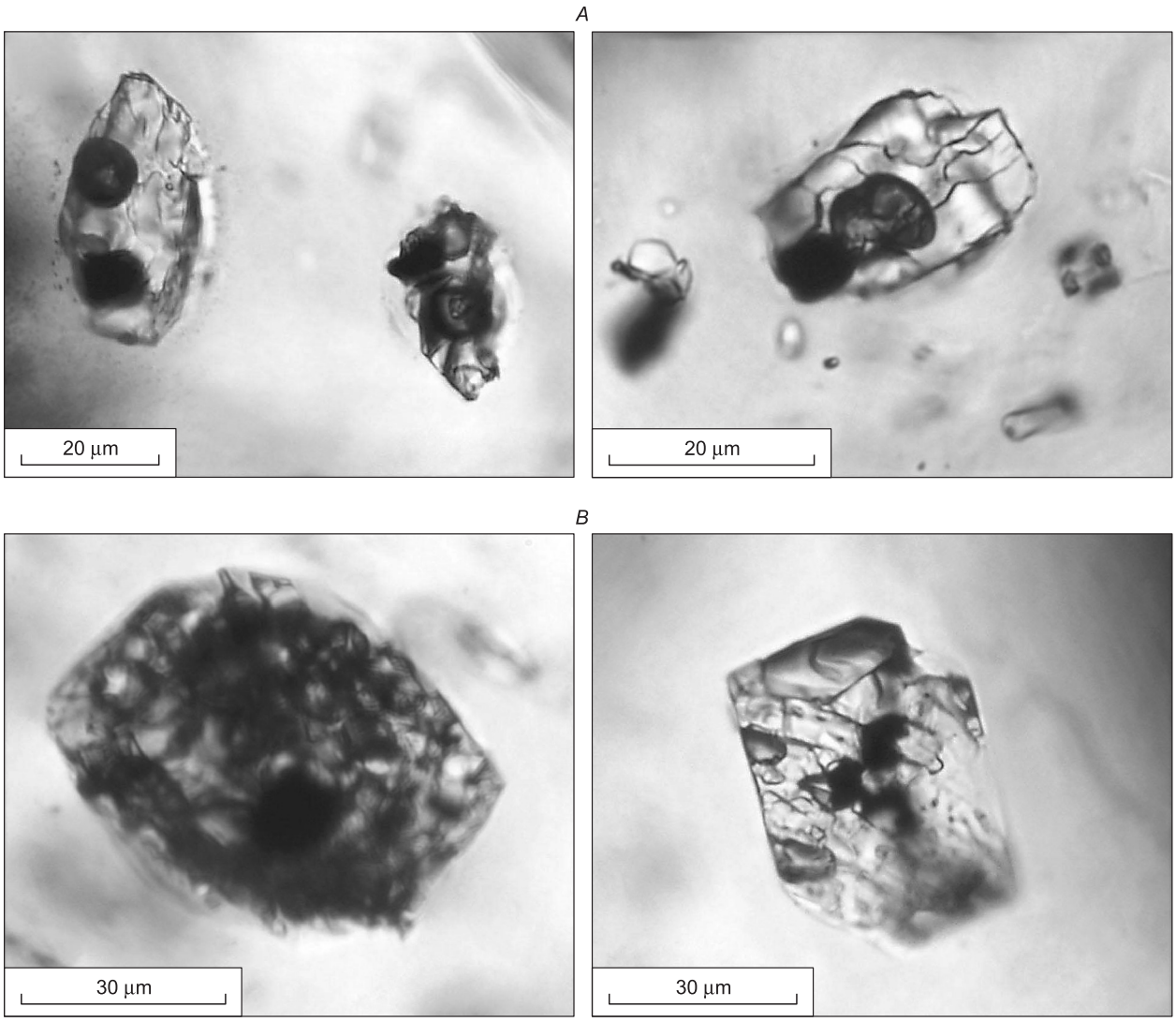

Fig. 10. Photographs of primary melt inclusions in clinopyroxene (*A*) and plagioclase (*B*) from Uksichan basalt.

chan lavas: decreasing Ti, Mg, and Ca oxides and increasing K_2O with SiO_2 increase. The inclusions in plagioclase and clinopyroxene form actually the same trend in the K_2O–SiO_2 diagram, which begins with the Uksichan basalts (including the K-15-16 sample studied in detail) and traces probable melt evolution paths during the formation of Middle Pliocene edifices at the base of Uksichan (Fig. 12).

Melt inclusions in clinopyroxene are generally similar to those in plagioclase in SiO_2, TiO_2, and CaO but differ in higher Mg and lower Na contents (Fig. 12). Note that almost

Table 6. Representative analyses of plagioclase phenocrysts from Uksichan basalt (wt.%), this study

No.	Analysis number and place	SiO_2	Al_2O_3	FeO	CaO	Na_2O	K_2O	Total	An
1	6	48.56	32.25	0.75	15.74	2.70	0.10	100.10	75.87
2	6a	52.28	29.55	0.86	12.68	4.43	0.20	100.00	60.57
3	8	52.23	29.78	0.88	12.99	3.92	0.20	100.00	63.92
4	9	47.98	32.41	0.93	16.31	2.37	0.10	100.10	78.72
5	10	47.20	33.16	0.74	16.65	2.16	0.09	100.00	80.57
6	11a	52.08	29.80	0.91	12.77	4.25	0.19	100.00	61.73
7	11b	50.56	30.90	0.69	13.93	3.78	0.15	100.01	66.50

Note. An is apfu content. Phenocrysts were 10–20 μm far from melt inclusions of any location.

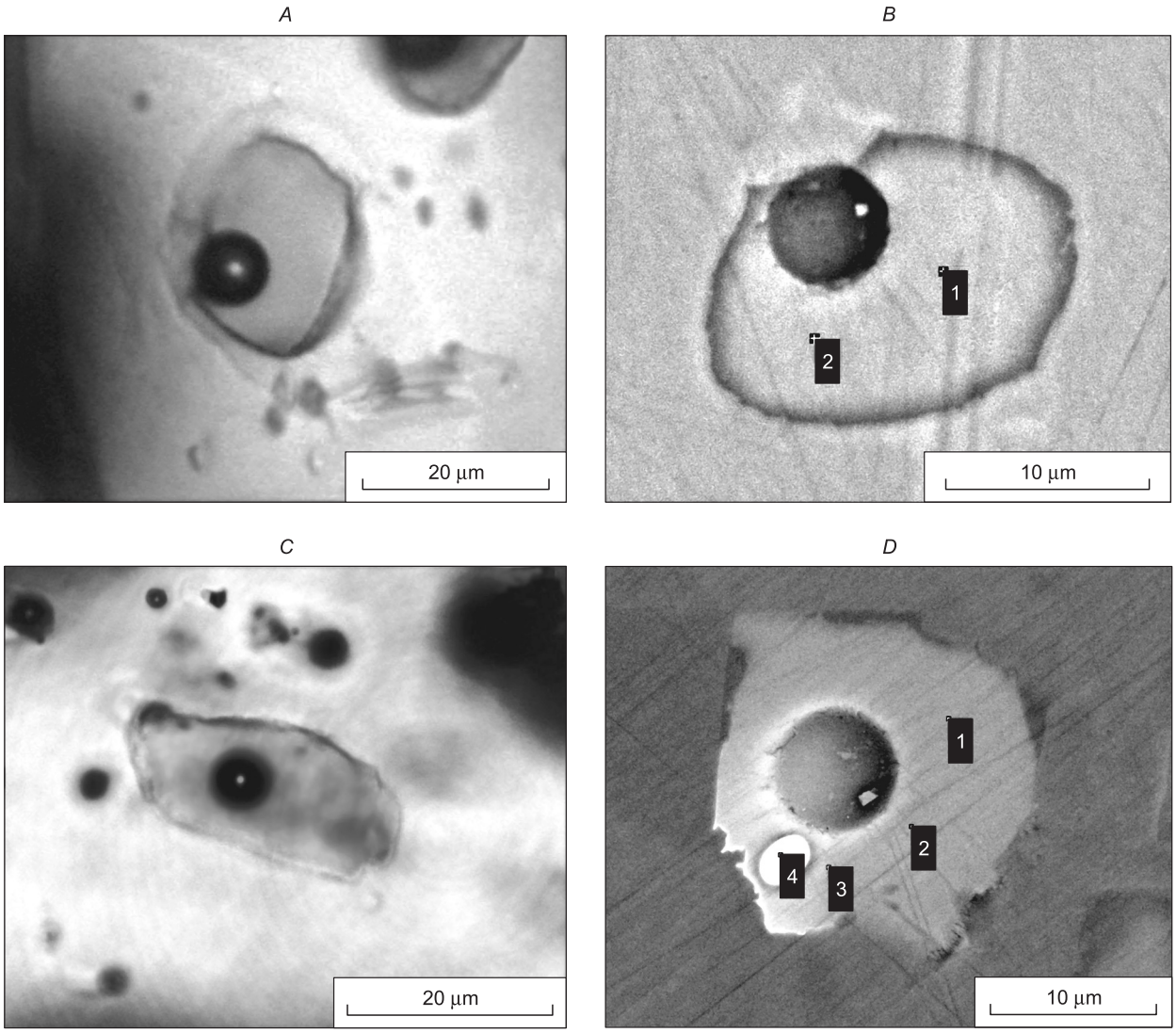

Fig. 11. Photographs of heated, homogenized, and quenched primary melt inclusions with homogeneous glass in clinopyroxene (*A*, *B*) and plagioclase (*C*, *D*) from Uksichan basalt. *B*, *D* are SEM images. Numerals show places of glass (1, 2, 3) and "ore drop" (4) analyses; ore drop contains 75 wt.% FeO and 20 wt.% TiO_2.

all diagrams in Fig. 12 show two parallel trends approaching, respectively, the upper and lower limits of fields for the Uksichan and Ichinsky lavas. In general, the melt inclusion compositions in the K-15-16 minerals are consistent with the evolution paths of the Uksichan lavas (especially, low-Ti inclusions in plagioclase), but inclusions in clinopyroxene have particular trends, possibly, because the sample represents the base of the volcano though being genetically related with the products of the following activity cycles.

The observed difference in the glass compositions in heated inclusions from plagioclase and clinopyroxene can be explained using the Al_2O_3–FeO/MgO diagram (Fig. 13) showing that the two minerals crystallized in different magmatic processes. Namely, plagioclase, which falls within the field of the Uksichan lavas, formed from fractionated residual melts with increasing FeO/MgO ratios, whereas clinopyroxene is related with the trend of cumulus pyroxene, with rapidly decreasing Al_2O_3 at almost stable Fe# (Fig. 13). The pyroxene cumulates proper have not been found, but the compositions of the inclusions indicate that the melt was prone to crystallize clinopyroxene, which happened in reality.

Only few homogeneous glasses of inclusions from orthopyroxene could be analyzed. The data record crystallization of orthopyroxene from calc-alkaline melts compositionally close to magnesian basaltic andesite (Fig. 12).

In general, melt inclusion data indicate that melt composition could vary considerably. Trend 1 (for basaltic and basaltic andesite melts, with ≤57 wt.% SiO_2) is prominent in the MgO–SiO_2 diagram of melt inclusions from clinopyroxene; trend 2 (for basaltic andesite melts, with ≤60 wt.% SiO_2) is marked by melt inclusions in plagioclase; trend 3 (for dacitic basalt melts, ≤64.5 wt.% SiO_2) is traceable by the compositions of rocks and melt inclusions in plagioclase (Fig. 12).

Table 7. Representative analyses of heated melt inclusions from Uksichan basalt (wt.%)

No.	Analysis number and place	SiO_2	TiO_2	Al_2O_3	FeO	MnO	MgO	CaO	Na_2O	K_2O	P_2O_5	Total	T_{hom}, °C
1	1a_ 3	52.74	1.36	10.21	12.47	0.42	6.79	10.70	2.59	0.53	N.d.	97.81	1215
2	1a_ 4	53.11	1.27	10.22	12.33	0.32	6.89	10.67	2.69	0.51	N.d.	98.01	1215
3	2_1	54.66	1.34	7.87	10.73	0.34	8.94	11.67	1.81	0.64	N.d.	98.00	1205
4	2_2	54.77	1.30	7.80	11.03	0.28	8.64	11.65	1.93	0.62	N.d.	98.02	1205
5	2_3	52.42	1.90	7.21	12.74	0.28	9.31	11.94	1.71	0.49	N.d.	98.00	1205
6	2_4	51.97	1.22	7.75	13.92	0.34	8.82	12.22	1.43	0.33	N.d.	98.00	1205
7	3_3	56.40	0.86	8.91	9.53	0.28	7.89	11.33	2.19	0.61	N.d.	98.00	1210
8	3_4	56.77	0.68	8.53	8.95	0.39	7.52	11.32	2.47	0.70	N.d.	97.33	1210
9	5_1	52.26	1.35	7.70	14.34	0.35	7.92	11.03	1.43	1.61	N.d.	97.99	1190
10	5_2	51.87	1.10	8.15	14.68	0.30	7.84	10.98	1.39	1.67	N.d.	97.98	1190
11	5_3	51.95	1.06	7.82	14.93	0.25	7.85	10.89	1.44	1.59	0.16	97.94	1190
12	5a_1	56.14	0.92	10.14	8.83	0.34	7.41	11.04	2.17	1.01	N.d.	98.00	1190
13	5a_2	55.47	1.09	10.15	9.10	0.22	7.48	11.42	2.17	0.90	N.d.	98.00	1190
14	5a_3	54.78	1.00	10.03	9.41	0.21	7.79	11.84	2.11	0.82	N.d.	97.99	1190
15	4_5	58.14	0.84	7.83	16.60	0.37	7.19	4.56	1.73	0.68	N.d.	97.94	1225
16	6_2	59.53	0.89	16.49	6.87	N.d.	2.48	7.99	4.60	0.94	0.21	100.00	1205
17	8_1	54.09	1.17	16.65	9.05	0.19	4.40	10.02	3.45	0.83	0.16	100.01	1175
18	8_2	54.39	1.17	16.69	8.92	N.d.	4.45	10.03	3.47	0.89	N.d.	100.01	1175
19	9_1	51.54	1.28	19.21	10.10	N.d.	4.12	8.78	3.98	0.65	0.35	100.01	1210
20	9_2	51.60	1.32	19.30	10.15	0.28	4.06	8.44	3.85	0.73	0.26	99.99	1210
21	9_3	47.83	1.54	16.66	12.91	0.29	6.46	8.73	2.45	0.87	0.28	98.02	1210
22	9_4	49.31	1.44	17.78	10.98	0.19	5.16	9.16	3.03	0.74	0.21	98.00	1210
23	10_1	55.42	0.85	15.61	8.63	0.17	3.85	9.34	4.48	0.80	0.40	99.55	1220
24	10_2	56.61	0.78	15.54	8.21	0.20	3.81	9.01	4.46	0.82	0.30	99.74	1220
25	10_3	56.24	1.73	15.73	8.91	0.17	3.50	9.49	3.27	0.76	0.21	100.01	1220
26	11a_1	58.77	1.21	18.73	5.25	N.d.	1.90	6.62	4.93	1.29	0.46	99.16	1200
27	11a_2	58.70	1.22	19.20	5.29	N.d.	1.94	6.80	4.82	1.32	0.23	99.52	1200
28	11b_1	54.89	1.46	17.36	8.89	0.00	3.14	8.92	4.32	0.80	0.21	99.99	1200
29	11b_2	55.07	1.25	17.59	8.64	N.d.	3.18	8.86	4.27	0.86	0.29	100.01	1200
30	11b_3	54.97	0.54	17.39	7.44	0.12	3.89	10.19	4.70	0.48	0.26	99.98	1200
31	11b_4	53.67	1.44	16.40	7.79	N.d.	4.61	10.81	4.21	0.50	0.21	99.64	1200
32	11b_5	53.76	1.29	18.85	9.59	0.20	2.39	7.44	4.52	1.73	N.d.	99.77	1200
33	10_4	51.72	2.13	15.62	9.47	0.39	4.63	8.87	4.62	0.65	0.63	98.73	1240

Note. Analyses are for homogeneous glasses that fill the whole volume (except gas bubble) of heated homogenized and quenched primary melt inclusions in clinopyroxene (1–14), orthopyroxene (15) and plagioclase (16–33) from Uksichan basalt (sample K-15-16). T_{hom} is the homogenization temperature; N.d., not determined.

Note in conclusion that comparative analysis of melt inclusions and lava compositions shows that most of major oxide contents in melt inclusions from plagioclase (with ≤1.5 wt.% TiO_2) coincide with those in the rocks (Figs. 12, 13) and, correspondingly, characterize features of magmatic systems of Uksichan volcano and their main evolution paths.

CRYSTALLIZATION OF MELTS IN INTERMEDIATE CHAMBERS

The data on primary melt inclusions were used to reconstruct the physicochemical parameters of magmatic systems in intermediate chambers beneath the Uksichan and Ichinsky Volcanoes, while the crystallization conditions were constrained by geothermobarometry. The results of clinopyroxene thermobarometers were checked against the melt inclusion data (see Methods). Modeling based on melt inclusions, as well as on pyroxene and amphibole chemistry, has provided insights into mineral-forming processes and evolution of magmatic systems during ascent of magma and crystallization of minerals in intermediate chambers.

Processing of the melt inclusion data (homogenization temperatures plus compositions of glasses after heating and quenching) with the *Petrolog* software (Danyushevsky and

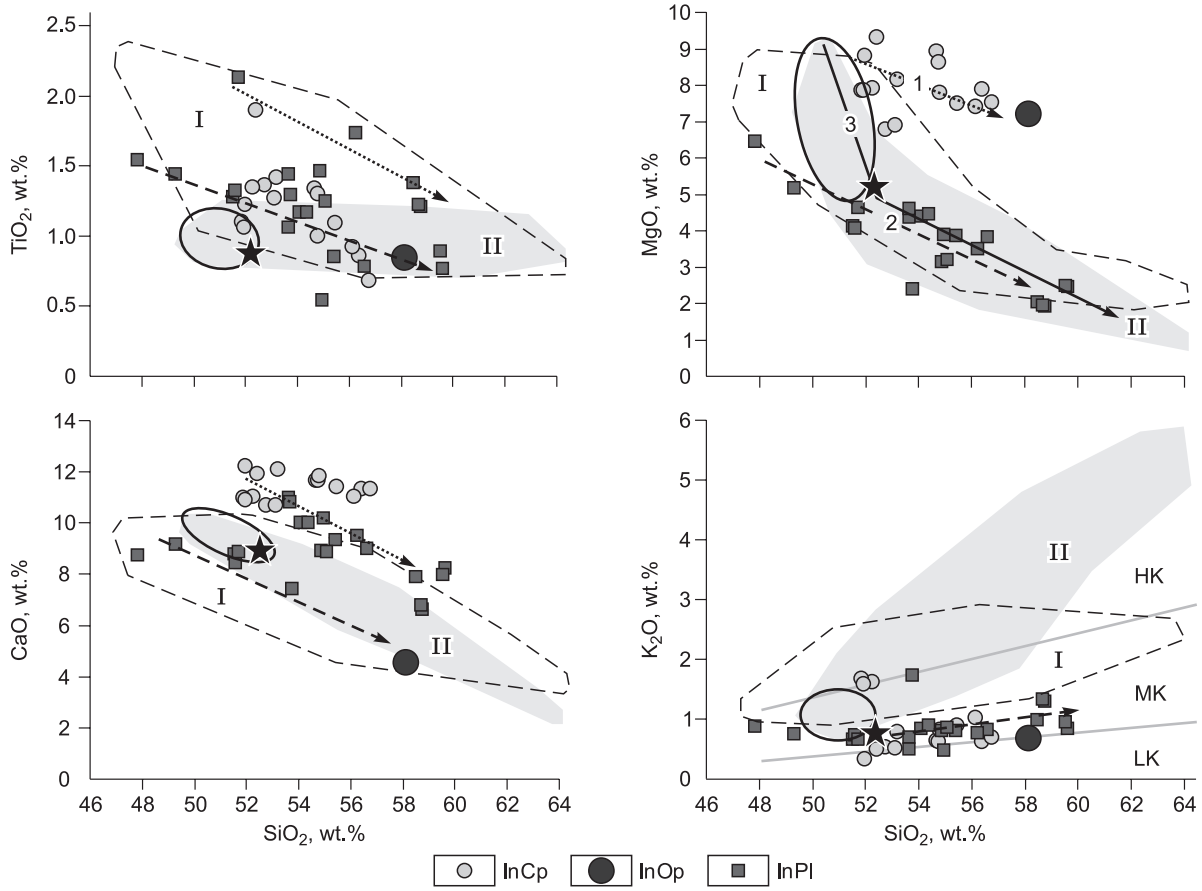

Fig. 12. Major oxide (wt.%) variation diagrams for heated homogenized melt inclusions in minerals from Uksichan basalt. InCp, InOp, InPl denote homogeneous glasses that fill the whole volume (except bubble) of homogenized melt inclusions in clinopyroxene (InCp), orthopyroxene (InOp) and plagioclase (InPl). Solid line contours moderately potassic Uksichan basalt, based on GEOROC database (http://georoc.mpch-mainz.gwdg.de/georoc/) and (Davydova, 2014). Asterisk marks sample K-15-16 from Uksichan. I and II are composition fields of Ichinsky (I) and Uksichan (II) lavas. Analyses of Ichinsky and Uksichan samples are from GEOROC database (http://georoc.mpch-mainz.gwdg.de/georoc/) and (Davydova, 2014). Dotted and dash lines are composition trends of inclusions with maximum and minimum values of components, respectively. 1, 2, 3 are melt evolution paths. LK, low-K series; MK, moderately K series; HK, high-K series, according (Bogatikov et al., 2009).

Plechov, 2011) yielded estimates of liquidus crystallization pressure for clinopyroxene and plagioclase in the Uksichan basalts. The obtained pressures correspond to four depth levels of crystallization: about 60, 45–30, 27–18 and from 12 km to near-surface (Fig. 14). The presence of four intermediate magma reservoirs is consistent with seismic tomographic images of subsurface beneath other Kamchatka volcanoes (Fig. 15). Both deep (~60 km) and shallow (10 km) sources revealed for Uksichan have their equivalents beneath the Tolbachik and Avachinsky Volcanoes revealed by seismic imaging.

The crystallization temperatures of the Uksichan minerals derived from melt inclusion data reach a maximum of 1320 °C in the deepest chambers (Fig. 14), or can be also lower (1215–1200 °C or even 1180 °C) at 60 to 50 km depths. Correspondingly, there are different *P–T* evolution paths of ascending melts. They may rise from 60 km, where they are the hottest (1320 °C), and cool down slowly upward to 1240–1215 and then to 1210–1175 °C, but accelerate from ~15 km and keep high temperatures of 1210–1200 °C. The originally cooler melts rise rapidly and preserve the temperatures they had at depths (Fig. 14).

The primary melts apparently originated near the top of slabs, about 100 km (Fig. 15) below the surface (Dobretsov et al., 2001, 2015) at temperatures no hotter than 1100–1200 °C. They heated up more or less strongly in the 100–60 km depth interval and cooled down between 60 and 20 km and shallower (Fig. 14).

The crystallization features of clinopyroxene and plagioclase vary with depth. Plagioclase formed at all four depth levels from 60 km to the surface, while clinopyroxene crystallized mainly between 21 and 18 km according to melt inclusion data or, possibly, together with plagioclase at greater depths of 45–60 km as indicated by calculations (Fig. 14).

The clinopyroxene geobarometry results agree well with the melt inclusion data and provide some additional knowledge. Specifically, they have confirmed the possibility of relatively low-temperature evolution of ascending melts and

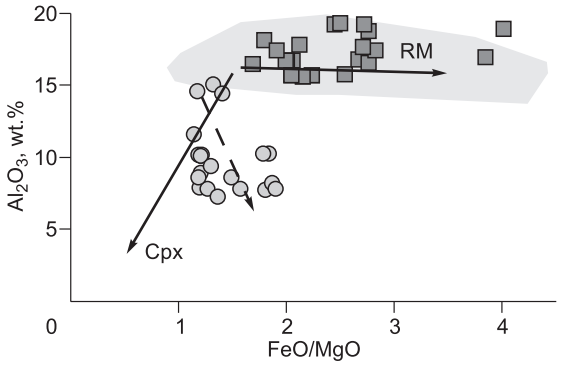

Fig. 13. Al_2O_3–FeO/MgO diagrams for heated homogenized melt inclusions in minerals from Uksichan basalt. Symbols are same as in Fig. 12. The field of Uksichan lavas (gray) is according to GEOROC database (http://georoc.mpch-mainz.gwdg.de/georoc/) and Davydova (2014). Solid line arrows are trends of cumulus clinopyroxene (Cpx) and residual melts (RM). Dash line is trend for inclusions in clinopyroxene. Diagram is based on this study and published data (Zolotukhin et al., 2003; Simonov et al., 2010, 2016).

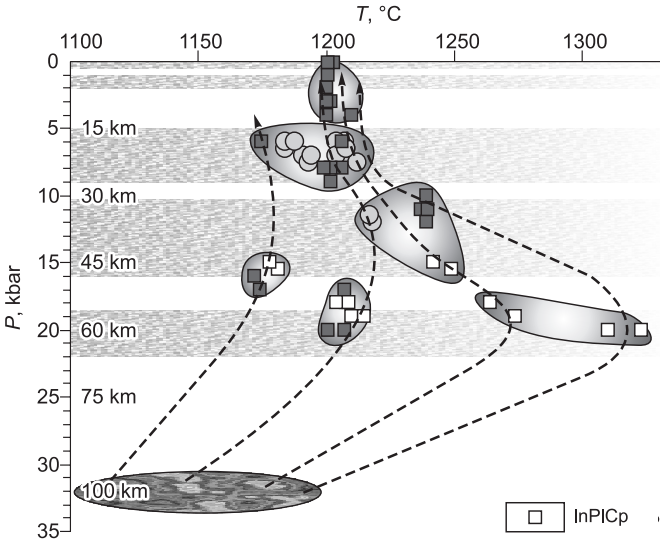

Fig. 14. Liquidus crystallization of clinopyroxene and plagioclase from Uksichan basalt (melt inclusion data): *P–T* diagram. InPlCp are crystallization conditions for clinopyroxene and syngenetic plagioclase. Other symbols are as in Fig. 12. Gray bands are depth levels of intermediate magma reservoirs beneath the Tolbachik and Avachinsky Volcanoes constrained by seismic data (Gontovaya et al., 2010; Dobretsov et al., 2016, 2017b) (Fig. 15). The field about 100 km is the inferred zone of parent melt generation. Dash lines are evolution paths of melts rising through intermediate chambers beneath Uksichan.

the presence of an intermediate chamber at 27–18 km, and revealed a larger temperature ridge of clinopyroxe crystallization in a shallow chamber (Fig. 16).

Thus, the data on melt inclusions and clinopyroxenes have implications for the *P–T* parameters of magma evolution with formation of clinopyroxene and plagioclase during the ascent of the melts through four intermediate chambers from the 60 km depth, where the crystallization temperature could reach 1320 °C, till eruption on the surface (Fig. 16).

As shown by previous studies (Dobretsov et al., 2016, 2017b), amphibole thermobarometry may provide information on *P–T* conditions in intermediate chambers beneath the Kamchatka volcanoes. Data of this kind were used to calculate pressures that existed during the formation of the Uksichan latite and dacite, as well as the Ichinsky andesite and dacite. They were as high as 5.5–7.5 kbar for amphibole in andesite (Ichinsky) and latite (Uksichan), as low as 1.0–3.4 kbar for amphibole in dacite from both volcanoes, and intermediate (3.5–5.2 kbar) for amphibole in dacite and andesite (Fig. 17); the highest and lowest estimates agree with those for other Kamchatka volcanoes.

Representative analyses of amphibole were used to compare the *P–T* parameters of the Ichinsky and Uksichan magmatic systems during the magma ascent. Crystallization occurred at three levels clearly detectable for both volcanoes (Fig. 18). Amphibole from the Ichinsky andesite began to crystallize at depths of 22.0–18.5 km and temperatures of 980–930 °C. That from the Uksichan latite formed at similar depths (18–16 km) but at higher temperatures of 1010–985 °C. Amphiboles from andesite and dacite of both volcanoes formed at shallower depths (15.5–11.0 km) and lower temperatures (945 to 880 °C), while dacitic amphiboles from both volcanoes crystallized at the final stage when the temperatures decreased to 900–810 °C and the depths reached 10 to 3 km. Thus, the evolution of the Ichinsky and Uksichan intermediate and felsic magmatic systems shared the same paths at the final low-temperature stage with crystallization in three intermediate chambers (Fig. 18).

Comparison of the melt inclusion results with clinopyroxene and amphibole compositions provides a comprehensive idea of the Uksichan magmatic system. The *P–T* trends of melts (Fig. 19) record their ascent from depths of ~ 60 km through several intermediate chambers, which generally agrees with seismic tomography images of magma reservoirs beneath the reference volcanoes of Kamchatka. The trend with maximum temperatures (up to 1350–1320 °C at 60 km and 1250–1180 °C in shallow subsurface) is traceable by melt inclusions and pyroxenes. The lower-temperature trend (1230–1200 °C at ~60 km and 1120 °C in the near-surface) appears mainly in melt inclusion data above 18 km and in clinopyroxene data from ~4 km. The evolution path of melts that originally had a temperature of 1180 °C at ~50 km branches at ~25 km, with the formation of clinopyroxene at 1100–1000 °C in a shallow chamber and amphibole at 1050–820 °C in a 18–6 km deep chamber, at a fluid pressure of 6–2 kbar (Fig. 19).

DISCUSSION

The evolution of the Uksichan magmatic systems was modeled previously (Davydova, 2014) in *Comagmat* (Ariskin et a1., 1993; Ariskin and Barmina, 2000; Kimura and Ariskin, 2014), using the results of geothermometry and

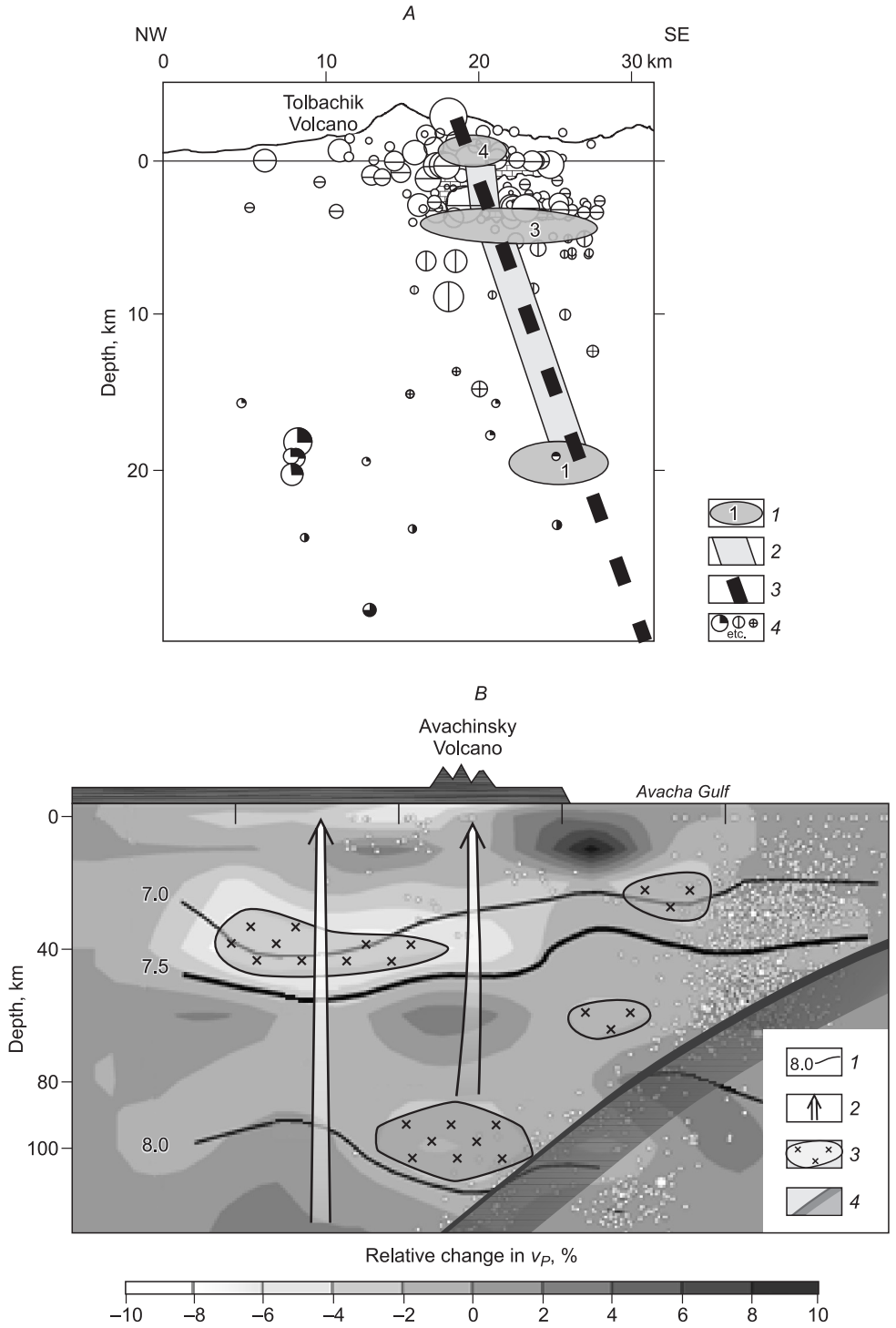

Fig. 15. Location of intermediate magma reservoirs beneath the Tolbachik and Avachinsky Volcanoes according to seismic data (Dobretsov et al., 2016, 2017b; Gontovaya et al., 2010). *A*, Tolbachik Volcano: *1*, magma reservoirs; *2*, paths of rising magma; *3*, deep fault; *4*, earthquakes of different origin depths and magnitudes (circle sizes are proportional to magnitudes). *B*, Avachinsky Volcano: *1*, *P*-wave velocity (v_P), km/s; *2*, melt migration paths; *3*, intermediate magma chambers; *4*, inferred slab top.

geobarometry by the method of Putirka (2008), taking into account Mg# in cores of olivine and partly clinopyroxene phenocrysts. However, Davydova (2014) did not use data on spinel, orthopyroxene, and amphibole, and on rims and microcrysts of olivine and clinopyroxene. We are bridging the gap in this study.

The Pliocene Uksichan lavas (Davydova, 2014) show the highest pressures and temperatures calculated as in (Putirka,

2008): 10.2–7.6 kbar and 1152–1123 °C on olivine and 8.4–5.7 kbar and 1148–1134 °C on clinopyroxene for moderately-Al samples; 9.8–8.1 kbar and 1116–1074 °C on olivine and 11–3.1 kbar and 1043–1060 °C for high-Al volcanics. The conditions for basalts from the field of cones are: 12 kbar and 1265 °C (on olivine). Pressures of 10–12 kbar and temperatures of 1150–1200 °C correspond to 25–30 km deep chambers at the crustal base (Fig. 20). Fitting of calculated mineral and rock composition trends attests to initial conditions of 21 kbar and 1300–1400 °C which existed in 50–60 km deep magma chambers where peridotitic mantle interacted with rising andesitic melts and/or equilibrated fluids (Dobretsov et al., 2015, 2016).

Our results for the Uksichan magmatic system agree with the estimates of Davydova (2014). Namely, calculations with our own melt inclusion data indicate that the crystallization temperature of minerals from the Uksichan lavas was the highest (1320 °C or more) at the deepest levels of 60–50 km and decreased progressively as magma was rising to the surface: 1320 → 1240 → 1200 °C. The trends with cooling from 1350–1320 °C at 60 km to 1250–1180 °C near the surface are traceable in both melt inclusion and pyroxene data. Our results showing the presence of an intermediate magma chamber in the 27–18 km interval (Figs. 16, 19) fit perfectly the *P–T* parameters of clinopyroxene crystallization calculated by Davydova (2014, Table 5.2 therein).

The reconstructed primary (Davydova, 2014) melts (Fig. 20) contain different amounts of water (2.5 and 1% H_2O for highly and moderately aluminous compositions, respectively), depending on the shares of interacting suprasubduction melts, fluids, and peridotite: high percentage of melt and fluid in the case of high-Al melts and predominance of peridotite at moderate Al contents.

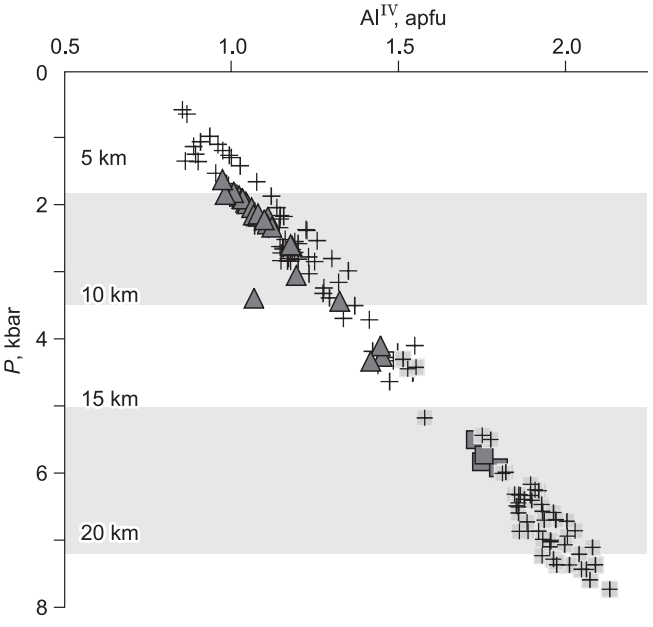

Fig. 17. Pressure-dependent variations of Al^{IV} (apfu) during crystallization of amphibole. Symbols are as in Fig. 8. Diagram is based on this study and published data on mineral compositions (Davydova, 2014; Dobretsov et al., 2016). Gray bands are pressure intervals for crystallization of amphibole from Bezymianny lavas (Kamchatka), after (Turner et al., 2007).

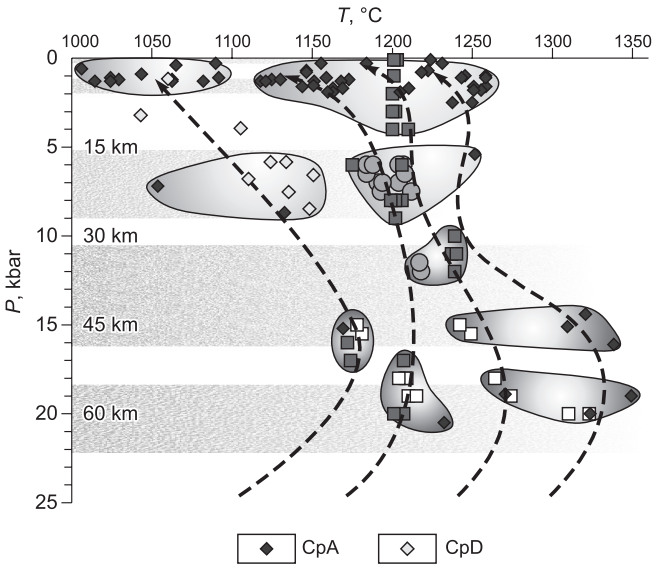

Fig. 16. Crystallization of clinopyroxene and plagioclase from basaltic melts in intermediate chambers beneath Uksichan (from data on melt inclusions and mineral thermobarometry). CpA are clinopyroxene barometry results of this study (see Methods) obtained using our analyses and data by Davydova (2014); CpD are clinopyroxene crystallization parameters calculated by Davydova (2014, Table 5.2 therein). Other symbols are as in Figs. 12 and 14.

The percentage of the Fo component is expected to reach 87–88% in olivine equilibrated with these melts and 92–93% in clinopyroxene, but the most magnesian olivine in the samples of Davydova (2014) contained 78–82% Fo (cores of phenocrysts), which corresponds to equilibrium at 25–30 km depths, in intermediate chambers at the crust base (Fig. 20).

The contents of CaO and MnO in magnesian olivine phenocrysts (Fig. 7) are as low as 0.2–0.35 and 0.3–0.5 wt.%, respectively, and increase as the Fo component decreases to >70%: to 1 wt.% MnO and 0.4 wt.% CaO in phenocrysts and rims, or occasionally up to 0.9 wt.% CaO in some microcrysts and rims. This behavior is possible in equilibrium with Ca-plagioclase upon fast quenching.

The analyzed clinopyroxene and orthopyroxene from the Uksichan samples have large ranges of CaO (Wo), TiO_2 and Al_2O_3 and plot between the 1200 and 1100 °C isotherms (Fig. 5). As Mg# decreases, Ca contents increase in orthopyroxene but decrease in clinopyroxene (Fig. 6).

The compositions of basalts and andesites from Q_3 shield volcanoes and Q_4 cones plot a single evolution trend (*C* and *D*, respectively, in Fig. 20) but the shield volcanoes (*C*) show predominant isobaric fractional crystallization at 10–15 km with decompression from 10 to 5 kbar while crystallization in the younger cones occurs during decompression

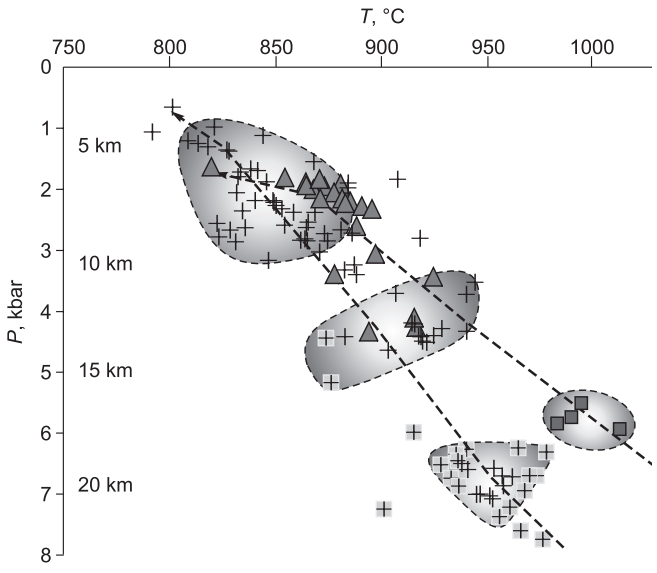

Fig. 18. Crystallization of amphibole from Ichinsky and Uksichan lavas in intermediate chambers: *P–T* diagram. Symbols are as in Fig. 8. Diagram is based on this study and published data on mineral compositions (Davydova, 2014; Dobretsov et al., 2016). Dash lines are evolution paths of melts rising through intermediate chambers beneath the Uksichan and Ichinsky Volcanoes.

from 10–19 kbar (30 km), at initial contents of 2.5 wt.% H_2O and the lowest decompression rate 0.25 kbar per 1% of crystallized material. The final result is close to successive or simultaneous crystallization of clinopyroxene, magmatite, and plagioclase.

The Quaternary basalts lost signatures of crystallization at 50–60 km, possibly, because they were hotter (~1400–1450 °C) than the Uksichan Al-basalt (1350 °C) at these depths as the suprasubduction temperature pattern had changed in the Holocene. Meanwhile, the formation of large homogeneous masses of basalt would be impossible otherwise, without a reaction of slab-derived fluids and melts with hot suprasubduction mantle.

The Uksichan lavas contain notably more potassium than those of Ichinsky and other volcanoes (see above). The origin of high-K basalt in subduction zones was discussed in many publications (Nikogosian et al., 2010; Lee et al., 2014; Portnyagin et al., 2015; Simakin et al., 2015; Dobretsov et al., 2017a; Gordeev and Dobretsov, 2017). High-K basalts are known from many places worldwide: shoshonite-latite basalts in the backarc part of the South American Cordillera; subduction-related K basalts in the zone of volcanic gases with high CO_2 in Italy (Frezzotti et al., 2009); lavas of the Klyuchevskoy group of volcanoes, including those of the Tolbachik fissure eruption (Portnyagin et al., 2015; Dobretsov et al., 2017a). However, the K_2O contents in the Tolbachik basalts are high (1.7–2.5 wt.%) only in the varieties with high Al (HAB) and 4–6 wt.% MgO, but are much lower in high-Mg basalts (HMB) containing >10 wt.% MgO. The HMB were inferred (Lukanin et al., 1980) to be of a deeper origin than HAB produced by fractional crystallization of magnesian basalts. This is unlikely for the Uksichan lavas though, as the HMB and HAB series show independent trends in the K_2O–SiO_2 (Fig. 4) and K_2O–MgO (Fig. 21) diagrams, as well as in the case of Tolbachik (Port-

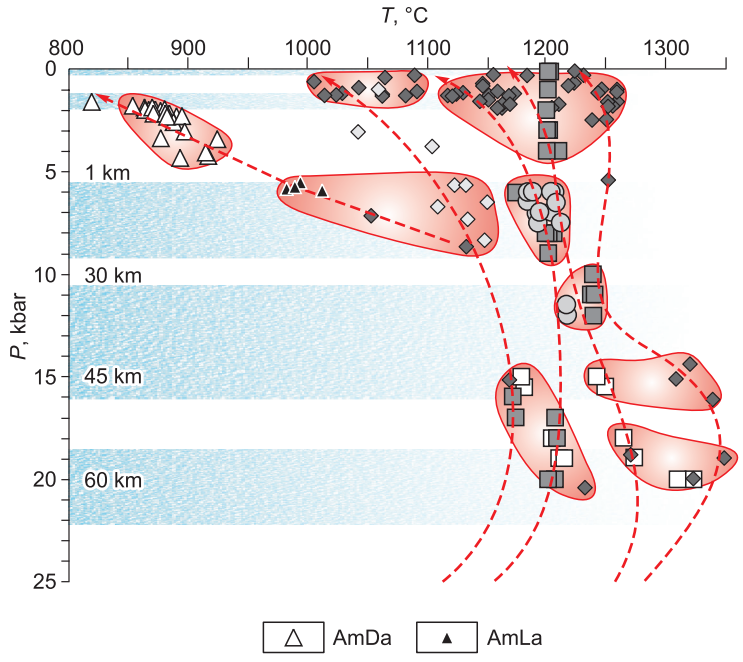

Fig. 19. Crystallization of minerals from Uksichan lavas in intermediate chambers: *P–T* diagram. AmDa, AmLa are data on amphibole from dacite (AmDa) and latite (AmLa). Other symbols are as in Figs. 12, 14, and 16. Blue bands are depth levels of intermediate magma reservoirs beneath the Tolbachik and Avachinsky Volcanoes according to seismic data (Gontovaya et al., 2010; Dobretsov et al., 2016, 2017b), as in (Fig. 15). Dash lines are evolution paths of melts rising through intermediate chambers beneath Uksichan.

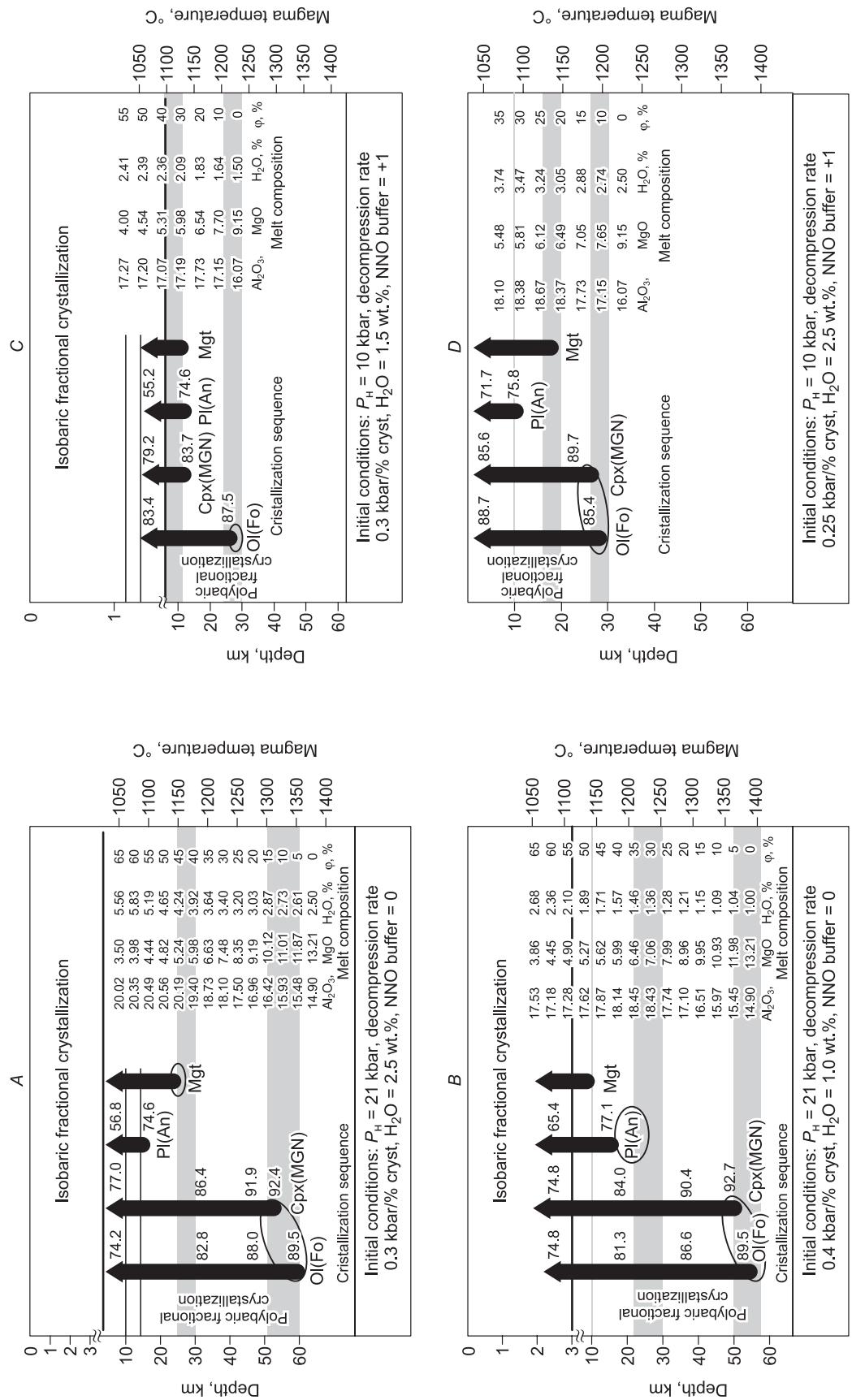

Fig. 20. Calculated P–T parameters of Uksichan magmatic systems. Models are based on data from Davydova (2014). *A*, high-Al rocks, N_2; *B*, moderately-Al rocks, N_2; *C*, Q_3 shield volcanic edifices; *D*, Q_4 small cones.

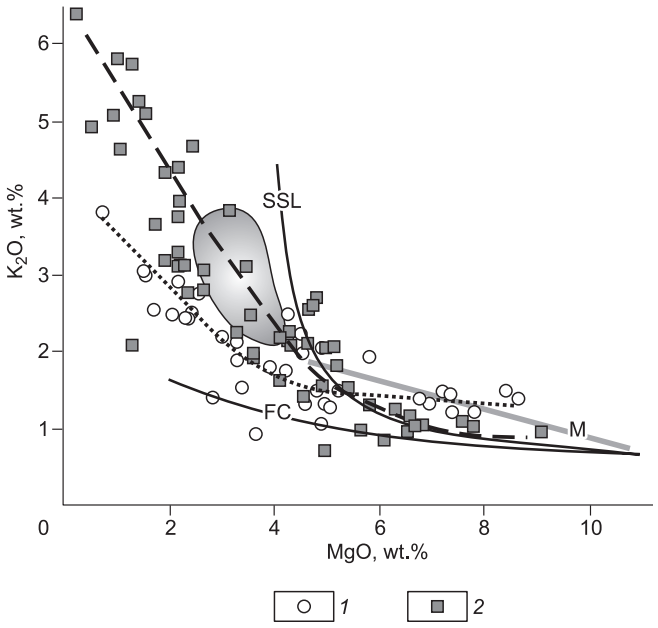

Fig. 21. K_2O–MgO diagram for crystallization in Ichinsky (*1*) and Uksichan (*2*) magmatic systems. Dotted and dash lines are, respectively, compositions of Ichinsky and Uksichan lavas. Abbreviations mark lines of crystallization conditions: FC, single step fractional crystallization; SSL, steady-state liquid crystallization of REFC melts (REFC, Recharge-Evacuation-Fractional Crystallization), M, mixing of highly magnesian and highly aluminous melts (HMB + HAB mixing). Gray fields correspond to REFC melts. Diagram is plotted with reference to published data (Portnyagin et al., 2015; Dobretsov et al., 2017a).

nyagin et al., 2015 and Figs. 8, 10 therein; Dobretsov et al., 2017a).

Melt inclusions in early-generation olivine xenocrysts with 88% Fo from the Tolbachik lavas enclose Ca–Ti–Mg garnet (melanite) with 30% of pyrope, K-carbonate, glass, and a gas phase (Simakin et al., 2015). Garnet formation corresponds to a pressure of 20–25 kbar (60–75 km depth), or to the conditions of the hottest magma chamber in the zone where hydrous andesite melts (or fluids) interact with mantle peridotite.

Glass in the analyzed melt inclusions from early olivine has a K-basaltic andesite composition (55–58 wt.% SiO_2, 1.4–3.5 wt.% MgO, and 2.5–6 wt.% K_2O), as well as in plagioclase and clinopyroxene (58 wt.% SiO_2, 2.9 wt.% MgO, and 3.15 wt.% K_2O), but clinopyroxene bears trachyandesitic glass (60–64 wt.% SiO_2, 0.6–1.2 wt.% MgO, and 3.0–4.5 wt.% K_2O). These data allow reconstructing a reaction between trachyandesite and peridotite (early Ol + Cpx) leading to the formation of K-HMB and basaltic andesite, as well as to fluid reduction to CH_4, CO_2, CO, and F_2 (Simakin et al., 2015) followed by magma mixing and fractional crystallization in shallow chambers.

The model in Fig. 21 combines mixing of high-Mg and high-Al melts (HMB + HAB mixing) and recharge-evacuation-fractional crystallization (REFC) according to Lee et al. (2014). This is an open magmatic system with multiple chambers, inputs and mixing of new batches of magma, and repeated fractional crystallization (Portnyagin et al., 2015). The trend for the Uksichan lavas almost coincides with the SSL line (steady state liquid crystallization of REFC melts) at MgO decreasing from 9 to 4.5 wt.% and crosses the REFC field at MgO decreasing from 4.5 to 2.6 wt.% and K_2O increasing from 2 to 3.6 wt.%. These data indicate that the Uksichan magmatic system is open and fractional crystallization predominates. The trend of the Ichinsky lavas coincides with the line of HMB + HAB mixing at MgO decreasing from 8.5 to 5.0 wt.% and then passes below REFC as MgO further lowers to 2 wt.%, unlike that for the Uksichan system.

CONCLUSIONS

1. The reported data from Uksichan and Ichinsky Volcanoes and the available published evidence have provided new insights into magmatism in the southwestern part of the Sredinnyi Ridge volcanic belt in Kamchatka.

2. Experimental results on melt inclusions show similar crystallization temperatures of minerals in the Uksichan Pliocene basaltic lavas: 1240–1175 °C for plagioclase, 1225–1180 °C for orthopyroxene, and 1215–1190 °C for clinopyroxene.

3. Modeling with reference to homogenization parameters of inclusions predicts that minerals in the Uksichan samples crystallized in intermediate magma chambers at different depths, which have been substantiated for the first time. The four chambers are located at the same depths (~60, 45–30, 27–18, and from 12 km to near-surface) as the magma reservoirs beneath other Kamchatka volcanoes detected by seismic tomography.

4. The crystallization temperatures retrieved from melt inclusion data may vary at the 60–50 km depths (1320 °C, 1215–1200 °C, and ~1180 °C) depending on the mantle thermal regime and record different evolution paths of ascending melts. The hottest magma (1320–1350 °C) rising from a depth of ~60 km cools down progressively (1320 → 1240 → 1200°C), while the originally lower-temperature magma ascends fast and preserves its initial temperatures. The latter inference is consistent with the fact that deep magma most often crystallizes and cools down below the surface.

5. Melt inclusion data, along with clinopyroxene and amphibole thermobarometry and mineral compositions, for the Uksichan samples reveals several trends of melts rising from 60 km through intermediate chambers. The highest-temperature trends (1350–1320 °C at the 60 km depth and 1250–1180 °C near the surface) are traceable from data on both melt inclusions and pyroxenes. The path of lower-temperature melts (1230–1200 °C at ~60 km to 1120 °C near the surface) is traceable mainly from melt inclusions to the depth 18 km and by clinopyroxene data upward since 4 km. The melts with the lowest temperatures of 1180 °C at ~50 km show a splitting trend above ~25 km: clinopyroxene

crystallizes at 1100–1000 °C in shallow sub-surface and amphibole forms at temperatures of 1050 to 820 °C and 6–2 kbar, or 18–6 km below the surface.

6. Representative data on amphibole compositions for the Uksichan and Ichinsky Volcanoes highlight the evolution of intermediate and felsic magmatic systems, with three levels of mineral crystallization in intermediate chambers: amphibole in the Ichinsky andesite and latite crystallized at 22.0–18.5 km (18–16 km) and 980–930 °C (1010–985 °C), respectively. Amphibole in andesite and dacite of both volcanoes crystallized jointly at shallower depths (15.5–11.0 km) and lower temperatures (945 to 880 °C). Only dacite-hosted amphibole from both volcanoes crystallized at the final stage, as the temperatures reached the 900–810 °C ridge while the melts rose from 10 to 3 km. The difference prompts melt ascent by different mechanisms, which requires further research.

The authors of the work express their gratitude to the professors A.B. Perepelov (A.P. Vinogradov Institute of Geochemistry SB RAS) and A.E. Izokh (V.S. Sobolev Institute of Geology and Mineralogy SB RAS) for constructive comments that helped improve the quality of the article.

The study was carried out as part of government assignment to the A.A. Trofimuk Institute of Petroleum Geology and Geophysics and contract No. 14.Y26.31.0029 supported by the Ministry of Science and Higher Education.

REFERENCES

Antipin, V.S., Volynets, O.N., Perepelov, A.B., Patoka, M.G., Uspensky, V.N., 1987. Geological relationships and geochemical evolution of Pliocene–Quaternary calc-alkaline and subalkaline magmatism of the Uksichan caldera, in: Geochemistry of Igneous Rocks in Modern and Pre-Cenozoic Active Zones [in Russian]. Nauka, Novosibirsk, pp. 72–81.

Ariskin, A.A., Barmina, G.S., 2000. Modeling Phase Equilibrium during Crystallization of Basaltc Magmas [in Russian]. Nauka/Interperiodika, Maik, Moscow.

Ariskin, A.A., Frenkel, M.Ya., Barmina, G.S., Nielsen, R.L., 1993. COMAGMAT: a Fortran program to model magma differentiation processes. Comp. Geosci. 19 (8), 1155–1170.

Bindeman, I.N., Ponomareva, V.V., Bailey, J.C., Valley, J.W., 2004. Volcanic arc of Kamchatka: a province with high-$\delta^{18}O$ magma sources and large-scale $^{18}O/^{16}O$ depletion of the upper crust. Geochim. Cosmochim. Acta 68 (4), 861–865.

Bindeman, I.N., Leonov, V.L., Izbekov, P.E., Ponomareva, V.V., Watts, K.E., Shipley, N.K., Perepelov, A.B., Bazanova, L.I., Jicha, B.R., Singer, B.S., Schmitt, A.K., Portnyagin, M.V., Chen, C.H., 2010. Large-volume silicic volcanism in Kamchatka, Ar–Ar and U–Pb ages, isotopic and geochemical characteristics of major pre-Holocene caldera-forming eruptions. J. Volcanol. Geotherm. Res. 189 (1–2), 57–80.

Bogatikov, O.A., (Ed.), 1983. Igneous Rocks. Book 1: Classification, Nomenclature, Petrography, Part 2 [in Russian]. Nauka, Moscow.

Bogatikov, O.A., Kovalenko, V.I. (Eds.), 1987. Igneous Rocks. Book 6: Evolution of Magmatism in the Earth's History [in Russian]. Nauka, Moscow.

Bogatikov, O.A., Petrov, O.V., Morozov, A.F. (Eds.), 2009. Petrographic Code of Russia [in Russian]. VSEGEI, St. Petersburg.

Danyushevsky, L.V., Plechov, P.Yu., 2011. Petrolog3: Integrated software for modeling crystallization processes. Geochem. Geophys. Geosystems 12 (7), Q07021.

Davydova, M.Yu., 2014. Origin and Evolution of Magmas in the Uksichan Volcanic Center (Sredinnyi Ridge, Kamchatka). PhD Thesis [in Russian]. TIG DVO RAN, Vladivostok.

Dobretsov, N.L., Kirdyashkin, A.G., Kirdyashkin, A.A., 2001. Mantle Geodynamics (second edition) [in Russian]. Izd. SO RAN, Novosibirsk.

Dobretsov, N.L., Koulakov, I.Yu., Polyansky, O.P., 2013. Geodynamics and stress-strain patterns in different tectonic settings. Russian Geology and Geophysics (Geologiya i Geofizika) 54 (4), 357–380 (469–499).

Dobretsov, N.L., Koulakov, I.Yu., Litasov, K.D., Kukarina, E.V., 2015. An integrate model of subduction: contributions from geology, experimental petrology, and seismic tomography. Russian Geology and Geophysics (Geologiya i Geofizika) 56 (1–2), 13–38 (21–55).

Dobretsov, N.L., Simonov, V.A., Kotlyarov, A.V., Kulakov, R.Yu., Karmanov, N.S., 2016. Physicochemical parameters of crystallization of melts in intermediate suprasubduction chambers (by the example of Tolbachik and Ichinskii Volcanoes, Kamchatka Peninsula). Russian Geology and Geophysics (Geologiya i Geofizika) 57 (7), 993–1015 (1265–1291).

Dobretsov, N.L., Gordeev, E.I., Koulakov, I.Yu., Simonov, V.A., 2017a. Zones of melting in a slab and intermediate chambers, in: Gordeev, E.I., Dobretsov, N.L. (Eds.), Tolbachk Fissure Eruption of 2012–2013 (TFE-50) [in Russian]. Izd. SO RAN, Novosibirsk, pp. 353–366.

Dobretsov, N.L., Simonov, V.A., Koulakov, I.Yu., Kotlyarov, A.V., 2017b. Migration of fluids and melts in subduction zones and general aspects of thermophysical modeling in geology. Russian Geology and Geophysics (Geologiya i Geofizika) 58 (5), 571–585 (701–722).

Fedotov, S.A., Masurenkov, Yu.P. (Eds.), 1991. Active Volcanoes of Kamchatka, Book 1 [in Russian]. Nauka, Moscow.

Frezzotti, M.L., Peccerillo, A., Panza, G., 2009. Carbonate metasomatism and CO_2 lithosphere–asthenosphere degassing beneath the Western Mediterranean: An integrated model arising from petrological and geophysical data. Chem. Geol. 262 (1–2), 108–120.

Godovikov, A.A., 1975. Mineralogy [in Russian]. Nedra, Moscow.

Gontovaya, L.I., Popruzhenko, S.V., Nizkous, I.V., 2010. Upper mantle structure in the ocean–continent transition zone in Kamchatka. Vulkanologiya i Seismologiya 4, 13–29.

Gordeev, E.I., Dobretsov, N.L. (Eds.), 2017. The Tolbachik Fissure Eruption of 2012–2013 (TFE-50) [in Russian]. Izd. SO RAN, Novosibirsk.

Johnson, M.C., Rutherford, M.J., 1989. Experimental calibration of the aluminium-in-hornblende geobarometer with application to Long Valley caldera (California) volcanic rocks. Geology 17 (9), 837–841.

Kimura, J.I., Ariskin, A.A., 2014. Calculation of water-bearing primary basalt and estimation of source mantle conditions beneath arcs: PRIMACALC2 model for WINDOWS. Geochem. Geophys. Geosyst. 15 (4), 1494–1514.

Kostitsyn, Yu., Anosova, M., 2013. U–Pb age of volcanic rocks in Uksichan caldera in the Sredinnyi Ridge of Kamchatka. Geokhimiya 51 (2), 171–179.

Kozhemyaka, N.N., 1995. Long-lasting volcanic centers in Kamchatka: types of edifices, lifespan, eruption volume, productivity, and mass balance. Vulkanologiya i Seismologiya 6, 3–19.

Kozhemyaka, N.N., 2001. Quaternary polygenetic volcanoes of Kamchatka: extent of volcanism, mass balance, intensity and productivity in specific types of edifices, volcanic zones, and region as a whole. Vulkanologiya i Seismologiya 5, 3–21.

Kutyev, F.Sh., 1975. Evolution of basaltic rocks in Kamchatka, in: Problems of Magmatism and Tectonics of the Russian Far East [in Russian]. Vladivostok, pp. 101–119.

Lavrenchuk, A.V., 2004. PLUTON software for calculating within-chamber differentiation of mafic magmas, in: Abstracts, 2nd Siberian Int. Conf. Young Geosci. [in Russian]. Novosibirsk. Gos. Univ. Novosibirsk, pp. 105–106.

Lavrent'ev, Yu.G., Karmanov, N.S., Usova, L.V., 2015. Electron probe microanalysis of minerals: Microanalyzer or scanning electron microscope? Russian Geology and Geophysics (Geologiya i Geofizika) 56 (8), 1154–1161 (1473–1482).

Lee, C.A., Lee, T.C., Wu, C.T., 2014. Modeling the compositional evolution of recharging, evacuating, and fractionating (REFC) magma chambers: Implication for differentiation of arc magmas. Geochim. Cosmochim. Acta 143, 8–22.

Lukanin, O.A., Kadik, A.A., Biggar, G.M., Fedotov, S.A., 1980. Physicochemical conditions for crystallization of basalts from the Great Tolbachik fissure eruption of 1975–1976. Vulkanologiya i Seismologiya 3, 16–50.

Melekestsev, I.V., Braitseva, O.V., Ponomareva, V.V., 2001. A new approach to the concept of an active volcano, in: Geodynamics and Volcanism of the Kuriles-Kamchatka Island Arc System [in Russian]. IViG DVO RAN, Petropavlovsk-Kamchatsky, pp. 191–203.

Mercier, J.C.C., 1980. Single-pyroxene thermobarometry. Tectonophysics 70 (1–2), 1–37.

Nikogosian, I.K., Manfred, J., van Bergen, M.J., 2010. Heterogeneous mantle source of potassium-rich magmas in central-southern Italy: Melt inclusion evidence from Roccamonfina and Ernici (Mid Latina Valley). J. Volcanol. Geotherm. Res. 197 (1–4), 279–302.

Nimis, P., Taylor, W.R., 2000. Single clinopyroxene thermobarometry for garnet peridotites. Part I. Calibration and testing of a Cr-in-Cpx barometer and an enstatite-in-Cpx thermometer. Contrib. Mineral. Petrol. 139 (5), 541–554.

Ogorodov, N.V., Kozhemiaka, N.N., Vazheevskaya, A.A., Ogorodova, A.S., 1972. Volcanoes and Quaternary Volcanism in the Sredinnyi Ridge of Kamchatka [in Russian]. Nauka, Moscow.

Perchuk, L.L., 1980. A pyroxene barometer and pyroxene geotherms. Dokl. AN SSSR 233 (6), 1196–2000.

Perepelov, A.B., 2004. Neogene–Quaternary shoshonite-latite magmatism of the Sredinnyi Ridge in Kamchatka: Tekletunup Volcano (geological history, petrography, mineralogy). Vulkanologiya i Seismologiya 3, 12–30.

Perepelov, A.B., 2005. Neogene–Quaternary shoshonite-latite magmatism in the Sredinnyi Ridge of Kamchatka: Tekletnup Volcano (geochemistry, petrology, tectonic setting). Vulkanologiya i Seismologiya 1, 22–36.

Perepelov, A.B., 2014. Cenozoic Magmatism in Kamchatka during Tectonic Setting Changes. DrSci Thesis [in Russian]. IGKh SO RAN, Irkutsk.

Perepelov, A.B., Puzankov, M.Yu., Ivanov, A.V., Filosofova, T.M., 2006. Basanites of Mt. Khukhch: First mineralogical-geochemical data on the Neogene K–Na alkaline magmatism in western Kamchatka. Dokl. Earth Sci. 409 (1), 765–768.

Perepelov, A.B., Shcherbakov, Yu.D., Chashchin, A.A., Puzankov, M. Yu., Karmanov, N.S., Tsypukova, S.S., 2016. Magnesian andesites of Kamchatka: geochemical types and formation conditions, in: Geological Processes Associated with Subduction, Collision, and Plate Sliding, Proc. 3rd All-Russ. Conf. Int. Contrib. [in Russian]. Dal'nauka, Vladivostok, pp. 200–204.

Pevzner, M.M., 2004. The first geological data on the chronology of Holocene eruptive activity in the Ichinskii Volcano (Sredinnyi Ridge, Kamchatka). Dokl. Earth Sci. 395A (3), 335–337.

Portnyagin, M., Duggen, S., Hauff, F., Mironov, N., Bindeman, I., Thirlwall, M., Hoernle, K., 2015. Geochemistry of the late Holocene rocks from the Tolbachik volcanic field, Kamchatka: Quantitative modeling of subduction-related open magmatic systems. J. Volcanol. Geoterm. Res. 307, 133–155.

Putirka, K.D., 2008. Thermometers and barometers for volcanic systems. Reviews in Miner. Geochem. 69(1), 61–120.

Putirka, K., Johnson, M., Kinzler, R., Longhi, J., Walker, D., 1996. Thermobarometry of mafic igneous rocks based on clinopyroxene-liquid equilibria, 0-30 kbar. Contrib. Mineral. Petrol. 123 (1), 92–108.

Ridolfi, F., Renzulli, A., 2012. Calcic amphiboles in calc-alkaline and alkaline magmas: thermobarometric and chemometric empirical equations valid up to 1130°C and 2.2 GPa. Contrib. Mineral. Petrol. 163(5), 877–895.

Schmidt, M.W., 1992. Amphibole composition as a function of pressure: an experimental calibration of the Al-in-hornblende barometer. Contrib. Mineral. Petrol. 110 (2-3), 304–310.

Simakin, A., Salova, T., Devyatova, V., Zelensky, M., 2015. Reduced carbonic fluid and possible nature of high-K magmas of Tolbachik. J. Volcanol. Geotherm. Res. 307, 210–221.

Simonov, V.A., 1993. Petrogenesis of Ophiolites: Evidence from Thermobarochemistry [in Russian]. OIGGM, Novosibirsk.

Simonov, V.A., Kotlyarov, A.V., 2016. Conditions of magma crystallization in intermediate chambers beneath Tolbachik and Ichinsky Volcanoes (Kamchatka): melt inclusion evidence, in: Proc. XVII All-Russ. Conf. Thermobarometry [in Russian]. BNTs SO RAN, Ulan-Ude, pp. 143–146.

Simonov, V.A., Safonova, I.Iu., Kovyazin, S.V., Kotliarov, A.V., 2010. Physico-chemical parameters of Neoproterozoic and Early Cambrian plume magmatism in the Paleo-Asian ocean (data on melt inclusions). Russian Geology and Geophysics (Geologiya i Geofizika) 51 (5), 507–520 (648–664).

Simonov, V.A., Kotlyarov, A.V., Stupakov, S.I., 2016. Formation conditions of paleooceanic basaltic complexes of the Kuznetsk Alatau, in: Correlation of Altaids and Uralids: Magmatism, Metamorphism, Stratigraphy, Geochronology, Geodynamics, and Metallogeny [in Russian]. Izd. SO RAN, Novosibirsk, pp. 176–178.

Sobolev, A.V., Slutskii, A.B., 1984. Composition and crystallization conditions of the initial melt of the Siberian meimechites in relation to the general problem of ultrabasic magmas. Geologiya i Geofizika (Soviet Geology and Geophysics) 25 (12), 97–109 (105–110).

Sobolev, A.V., Danyushevsky, L.V., 1994. Petrology and geochemistry of boninites from the north termination of the Tonga Trench: Constraints on the generation conditions of primary high-Ca boninite magmas. J. Petrol. 35 (5), 1183–1211.

Stefanov, Yu.M., Shirokii, B.I., 1980. Upper Crust Metallogeny of Kamchatka [in Russian]. Nauka, Moscow.

Turner, S.P., Sims, K.W.W., Reagan, M.K., Cook, C., 2007. A ^{210}Pb–^{226}Ra–^{230}Th–^{238}U study of Klyuchevskoy and Bezymianny volcanoes, Kamchatka. Geochim. Cosmochim. Acta 71 (19), 4771–4785.

Yavuz, F., 2007. WinAmphcal: A Windows program for the IMA-04 amphibole classification. Geochem. Geophys. Geosystems 8 (1), Q01004.

Zolotukhin, V.V., Simonov, V.A., Al'mukhamedov, A.I., Medvedev, A. Yu., Vasil'ev, Yu.R., 2003. Comparative analysis of continental and oceanic plateau basalts (data on the Siberian Platform and Ontong Java Plateau). Geologiya i Geofizika (Russian Geology and Geophysics) 44 (12), 1339–1348 (1293–1302).

Editorial responsibility: A.E. Izokh